SCISPACE
formerly Typeset

Open access • Journal Article • DOI:10.1007/S10444-013-9338-8

Algebraic-Trigonometric Pythagorean-Hodograph curves and their use for Hermite interpolation — Source link

Lucia Romani, Laura Saini, Gudrun Albrecht

Institutions: University of Milan, university of lille

Published on: 01 Dec 2014 - Advances in Computational Mathematics (Springer US)

Topics: Hermite interpolation, Cubic Hermite spline, Trigonometric functions, Quintic function and Hermite polynomials

Related papers:

- Pythagorean-Hodograph Curves: Algebra and Geometry Inseparable
- Hermite interpolation by Pythagorean hodograph quintics
- Optimal bases for a class of mixed spaces and their associated spline spaces
- Pythagorean hodographs
- Hermite Interpolation by Rotation-Invariant Spatial Pythagorean-Hodograph Curves

Share this paper:

View more about this paper here: https://typeset.io/papers/algebraic-trigonometric-pythagorean-hodograph-curves-and-3tdxwgv1r3

Noname manuscript No.
(will be inserted by the editor)

Algebraic-Trigonometric Pythagorean-Hodograph curves and their use for Hermite interpolation

Lucia Romani · Laura Saini · Gudrun Albrecht

Received: date / Accepted: date

Abstract In this article we define a new class of Pythagorean-Hodograph curves built-upon a six-dimensional mixed algebraic-trigonometric space, we show their fundamental properties and compare them with their well-known quintic polynomial counterpart. A complex representation for these curves is introduced and constructive approaches are provided to solve different application problems, such as interpolating C^1 Hermite data and constructing spirals as G^2 transition elements between a line segment and a circle, as well as between a pair of external circles.

Keywords Pythagorean Hodograph · Trigonometric functions · Generalized Bézier curves · Hermite interpolation · G^2 transition elements · Spirals

Mathematics Subject Classification (2000) 65D05 · 65D07 · 65D17 · 41A30 · 41A05

1 Introduction and motivations

The purpose of this article is to investigate the existence of planar, trigonometric Pythagorean Hodograph curves defined over a mixed algebraic–trigonometric space possessing a normalized B–basis. These curves are shown to be the analogue of the polynomial Pythagorean–Hodograph (PH) quintics in the considered non-polynomial space - due to the fact that they enjoy an analogous property on the hodograph - and are thus called Algebraic-Trigonometric Pythagorean-Hodograph (ATPH) curves. Their planar polynomial counterpart was originally introduced by Farouki and Sakkalis in [3]. These curves, commonly called PH curves since the Euclidean norm of their hodograph is also a polynomial, have the useful properties of admitting a closed–form polynomial representation of their arc–length as well as exact rational parameterizations of their offset curves. Since their introduction they have widely been investigated mainly for solving practical problems from applications that particularly benefit from the PH curves' particular properties. Rational and spatial counterparts of polynomial PH curves have as well been proposed, but we are not aware of any attempts of defining Pythagorean Hodograph curves over a mixed algebraic–trigonometric space. This observation motivated us to expand the boundary of the PH curve theory into the realm of non-polynomial curves, in order to show that the benefits of polynomial PH curves over generic polynomial curves can be extended also to curves defined over more complicated function spaces. The function spaces we consider are the Algebraic-Trigonometric (AT) spaces deeply investigated in [2,14–16], since they offer the advantage of providing an exact description of a wide variety of trigonometric curves, such as, e.g., ellipses, lemniscates, cardioids, and others. In fact, we believe the extension of the PH property from parametric polynomial curves to parametric

L. Romani
Dip. di Matematica e Applicazioni, Università di Milano-Bicocca, Via R. Cozzi 53, 20125 Milano, Italy
Tel.: +39-0264485735, Fax: +39-0264485705, E-mail: lucia.romani@unimib.it

L. Saini, G. Albrecht
UNIV Lille Nord de France, UVHC, LAMAV-CGAO, FR no.2956, F-59313, Valenciennes, France
E-mail: Laura.Saini@univ-valenciennes.fr, Gudrun.Albrecht@univ-valenciennes.fr

curves defined over a mixed algebraic-trigonometric space beneficial to augmenting the flexibility of the important class of PH curves in curve design. This new class of ATPH curves should therefore be seen as a beneficial addition to the existing polynomial PH curves in the same way as general AT curves complement general polynomial curves. In fact, this new subclass of AT curves inherits a closed form representation of their arc–length and a rational algebraic-trigonometric representation of the curve's offsets. In this article we show how ATPH curves can be conveniently used to solve different Hermite interpolation problems. For this purpose we revisit several important publications, such as [5, 6, 11, 12], dealing with the solution of analogous problems by polynomial PH curves, in order to generalize them to our non-polynomial context. In particular, while [5] and [12] solve the C^1 Hermite interpolation problem by polynomial PH quintics and analyze the shape of the obtained solutions, [6] and [11] consider the problem of joining G^2–continuously basic elements such as line segments and circles by polynomial PH quintics of monotone curvature, also referred to as PH spirals. As also done in [4–6, 12] for polynomial PH curves, to facilitate the solution of the above Hermite problems a complex representation of the novel class of ATPH curves is used, and a general constructive approach exploiting their key properties is proposed.
The remainder of the article is organized as follows. In Section 2 we recall some known results on normalized B–bases of pure trigonometric and mixed algebraic–trigonometric spaces. Section 3 considers generalized Bézier curves defined over a six–dimensional algebraic–trigonometric space, shows their capability of reproducing well–known trigonometric curves and proposes a de Casteljau-like algorithm for their exact and stable evaluation. Section 4 is dedicated to the definition and construction of ATPH curves generalizing polynomial PH quintics. These curves have the property that the Euclidean norm of their hodograph is a trigonometric function, their arc-length is a mixed algebraic–trigonometric function and their unit tangent, unit normal as well as signed curvature are described by rational trigonometric functions. In Section 5 the class of ATPH curves is employed to solve the C^1 Hermite interpolation problem. The obtained four solutions are analyzed and the best one is identified. Section 6 deals with the construction of ATPH curves with monotone curvature, also called ATPH spirals, for joining G^2-continuously a line segment and a circle as well as two external circles. In both cases the obtained solutions turn out to be more flexible than their polynomial PH counterparts, thanks to the additional shape parameter offered by the ATPH representation. Conclusions are drawn in Section 7.

2 Normalized B-bases for pure trigonometric and mixed algebraic–trigonometric spaces

Let $t \in [0, \alpha]$ and $0 < \alpha < \pi$. For an arbitrary $m \in \mathbb{N}$ we consider the space of order m trigonometric polynomials

$$\tilde{U}_{2m} = \langle 1, \{\sin(\ell t), \cos(\ell t)\}_{\ell=1}^{m} \rangle,$$

and we denote by

$$\tilde{B}_i^{2m}(t) = \binom{2m}{i} \mu_i \left(\frac{\cos\left(\frac{2t-\alpha}{4}\right)}{\cos\left(\frac{\alpha}{4}\right)} \right)^{2m} \left(\frac{1}{2} + \frac{\tan\left(\frac{2t-\alpha}{4}\right)}{2\tan\left(\frac{\alpha}{4}\right)} \right)^{i} \left(\frac{1}{2} - \frac{\tan\left(\frac{2t-\alpha}{4}\right)}{2\tan\left(\frac{\alpha}{4}\right)} \right)^{2m-i}, \qquad i = 0, ..., 2m,$$

with

$$\mu_i \equiv \mu_{2m-i} := \binom{2m}{i}^{-1} \sum_{r=0}^{\lfloor i/2 \rfloor} \binom{m}{i-r} \binom{i-r}{r} \left(2\cos\left(\frac{\alpha}{2}\right)\right)^{i-2r}, \qquad i = 0, ..., m, \tag{1}$$

the normalized B-basis proposed in [17] for such a space. Note that, since $0 < \alpha < \pi$, then for any choice of α in that range the μ_i are strictly positive values. Moreover, as pointed out in [17], the basis functions $\tilde{B}_i^{2m}$, $i = 0, ..., 2m$ possess the following properties:

(i) Symmetry: $\tilde{B}_i^{2m}(t) = \tilde{B}_{2m-i}^{2m}(\alpha - t),\ t \in [0, \alpha]$;
(ii) Positivity: $\tilde{B}_i^{2m}(t) \geq 0,\ t \in [0, \alpha]$;
(iii) Partition of unity: $\sum_{i=0}^{2m} \tilde{B}_i^{2m}(t) = 1,\ t \in [0, \alpha]$;
(iv) Recursion: $\tilde{B}_i^{2m} = \tilde{B}_0^2\, \tilde{B}_i^{2(m-1)} + \tilde{B}_1^2\, \tilde{B}_{i-1}^{2(m-1)} + \tilde{B}_2^2\, \tilde{B}_{i-2}^{2(m-1)},\ \ m \geq 2\,.$

The functions $\tilde{B}_i^{2m}(t)$, $i = 0, ..., 2m$ can be regarded as the true equivalent of the Bernstein polynomials in $\tilde{U}_{2m}$, and they tend to the ordinary Bernstein polynomials of degree $2m$ whenever $\alpha \to 0$. On the

other hand, note that the parameter α, if progressively increased in its range of definition, offers an interesting tension-like effect (see Figure 1 (a)-(c)) and, when approaching π, only the first and the last functions of the normalized B-basis $\tilde{B}_i^{2m}$, $i = 0, ..., 2m$ are non-vanishing. Therefore the associated curve $\mathbf{x}(t) = \sum_{i=0}^{2m} \mathbf{p}_i \tilde{B}_i^{2m}(t)$, $t \in [0, \alpha]$ degenerates to the segment $\mathbf{p}_0\mathbf{p}_{2m}$. For instance, when $\alpha \to \pi$, the normalized B-basis $\tilde{B}_i^2$, $i = 0, 1, 2$ for the space $\tilde{U}_2 = \langle 1, \sin(t), \cos(t)\rangle$ assumes the following form

$$\lim_{\alpha\to\pi} \tilde{B}_0^2(t) = \frac{1}{2}(1 + \cos(t)), \qquad \lim_{\alpha\to\pi} \tilde{B}_1^2(t) = 0, \qquad \lim_{\alpha\to\pi} \tilde{B}_2^2(t) = \frac{1}{2}(1 - \cos(t)).$$

This limit case is illustrated in Figure 1(d).

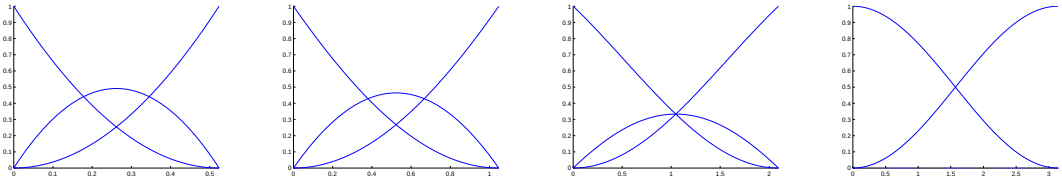

(a) (b) (c) (d)

Fig. 1 Basis functions $\tilde{B}_i^2(t)$, $i = 0, 1, 2$ for $t \in [0, \alpha]$ and $\alpha = \frac{\pi}{6}$ (a), $\alpha = \frac{\pi}{3}$ (b), $\alpha = \frac{2}{3}\pi$ (c), $\alpha \to \pi$ (d).

For later use we give the explicit expressions of the normalized B-bases for the spaces $\tilde{U}_2$, $\tilde{U}_4$ and $\tilde{U}_6$, hereinafter denoted by $\{\tilde{B}_i^2\}_{i=0,1,2}$, $\{\tilde{B}_i^4\}_{i=0,\cdots,4}$, $\{\tilde{B}_i^6\}_{i=0,\cdots,6}$, respectively:

$$\begin{aligned}
\tilde{B}_0^2(t) &= \tfrac{\cos(\alpha-t)-1}{\cos(\alpha)-1},\\
\tilde{B}_1^2(t) &= \tfrac{\cos(\alpha)-\cos(t)-\cos(\alpha-t)+1}{\cos(\alpha)-1},\\
\tilde{B}_2^2(t) &= \tfrac{\cos(t)-1}{\cos(\alpha)-1},
\end{aligned}$$

$$\begin{aligned}
\tilde{B}_0^4(t) &= \tfrac{(\cos(\alpha-t)-1)^2}{(\cos(\alpha)-1)^2},\\
\tilde{B}_1^4(t) &= \tfrac{2(\cos(\alpha-t)-1)(\cos(\alpha)-\cos(t)-\cos(\alpha-t)+1)}{(\cos(\alpha)-1)^2},\\
\tilde{B}_2^4(t) &= \tfrac{2(\cos(\alpha-t)-1)(\cos(t)-1)+(\cos(\alpha)-\cos(t)-\cos(\alpha-t)+1)^2}{(\cos(\alpha)-1)^2},\\
\tilde{B}_3^4(t) &= \tfrac{2(\cos(t)-1)(\cos(\alpha)-\cos(t)-\cos(\alpha-t)+1)}{(\cos(\alpha)-1)^2},\\
\tilde{B}_4^4(t) &= \tfrac{(\cos(t)-1)^2}{(\cos(\alpha)-1)^2},
\end{aligned} \tag{2}$$

$$\begin{aligned}
\tilde{B}_0^6(t) &= \tfrac{(\cos(\alpha-t)-1)^3}{(\cos(\alpha)-1)^3},\\
\tilde{B}_1^6(t) &= \tfrac{-48\cos(\alpha/2)\sin(t/2)\sin(\alpha/2-t/2)^5}{(\cos(\alpha)-1)^3},\\
\tilde{B}_2^6(t) &= \tfrac{3\,(2\cos(\alpha)+3)(\cos(t)-1)(\cos(\alpha-t)-1)^2}{(\cos(\alpha)-1)^3},\\
\tilde{B}_3^6(t) &= \tfrac{-32\sin(t/2)^3\sin(\alpha/2-t/2)^3\cos(\alpha/2)(\cos(\alpha)+4)}{(\cos(\alpha)-1)^3},\\
\tilde{B}_4^6(t) &= \tfrac{3\,(2\cos(\alpha)+3)(\cos(t)-1)^2(\cos(\alpha-t)-1)}{(\cos(\alpha)-1)^3},\\
\tilde{B}_5^6(t) &= \tfrac{-48\cos(\alpha/2)\sin(t/2)^5\sin(\alpha/2-t/2)}{(\cos(\alpha)-1)^3},\\
\tilde{B}_6^6(t) &= \tfrac{(\cos(t)-1)^3}{(\cos(\alpha)-1)^3}.
\end{aligned}$$

Moreover, we also recall the *de Casteljau-like algorithm* presented in [15] for evaluating trigonometric Bézier curves over the space $\tilde{U}_2$. Given a trigonometric Bézier curve $\mathbf{x}(t) = \sum_{i=0}^{2} \mathbf{p}_i^0 \tilde{B}_i^2(t)$, its evaluation at an arbitrary parameter value $t \in [0, \alpha]$, $0 < \alpha < \pi$, is obtained by the following corner cutting algorithm

$$\begin{aligned}
\mathbf{p}_0^1 &= (1 - \lambda_0^0(t))\mathbf{p}_0^0 + \lambda_0^0(t)\mathbf{p}_1^0,\\
\mathbf{p}_1^1 &= (1 - \lambda_1^0(t))\mathbf{p}_1^0 + \lambda_1^0(t)\mathbf{p}_2^0,\\
\mathbf{p}_0^2 &= (1 - \lambda_0^1(t))\mathbf{p}_0^1 + \lambda_0^1(t)\mathbf{p}_1^1,
\end{aligned} \tag{3}$$

where

$$\lambda_0^0(t) = \tfrac{\sin(\alpha)\,(\cos(t)-1)}{\sin(t)\,(\cos(\alpha)-1)}\,,$$
$$\lambda_1^0(t) = \tfrac{\cos(t)-\cos(\alpha)+\cos(\alpha-t)-1}{\sin(\alpha-t)\,\sin(\alpha)}\,, \qquad \text{such that} \quad \mathbf{x}(t) = \mathbf{p}_0^2.$$
$$\lambda_0^1(t) = \tfrac{\sin(\alpha-t)(\cos(t)-1)}{\sin(\alpha)-\sin(t)-\sin(\alpha-t)}\,,$$

In Figure 2 we illustrate an application example of the de Casteljau-like algorithm to subdivide the trigonometric Bézier curve $\mathbf{x}(t)$ with $\alpha = \frac{\pi}{2}$ at a given parameter $t \in [0, \alpha]$.

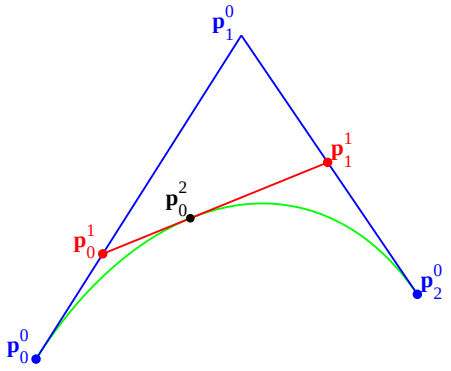

Fig. 2 Subdivision of a trigonometric Bézier curve in $\tilde{U}_2$ with $\alpha = \frac{\pi}{2}$ at the parameter $t = \frac{\pi}{5} \in [0, \alpha]$.

So far, we have focussed our attention on normalized B-bases of pure trigonometric spaces. We conclude this section by recalling some results from the articles [14] and [16] about normalized B-bases of algebraic-trigonometric spaces. In particular, in [14] a normalized B-basis of the mixed linear-trigonometric functional space

$$U_5 = \langle 1,\, t,\, \sin(t),\, \cos(t),\, \sin(2t),\, \cos(2t)\rangle,$$

hereinafter denoted by $\{B_i^5(t)\}_{i=0,\dots,5}$, is presented for $t \in [0, \alpha]$ and $0 < \alpha < 2\pi$. Introducing the notation

$$s_1 = \sin(\tfrac{\alpha}{2}), \quad c_1 = \cos(\tfrac{\alpha}{2}), \quad s_2 = \sin(\alpha), \quad c_2 = \cos(\alpha), \tag{4}$$

and the abbreviations

$$n_0 = 6\alpha + 2s_2(c_2 - 4), \quad n_1 = c_1(s_2 - 3\alpha) + 4s_1, \quad n_2 = (2 + c_2)\alpha - 3s_2, \tag{5}$$

the normalized B-basis of U_5 can be written using the explicit expressions

$$\begin{aligned}
B_0^5(t) &= \tfrac{2}{n_0}\Big(3(\alpha - t) + \sin(\alpha - t)\,(\cos(\alpha - t) - 4)\Big),\\
B_1^5(t) &= \tfrac{4s_1}{n_0 n_1}\Big(n_0 \sin^4\big(\tfrac{\alpha - t}{2}\big) - 2s_1^4\big(3(\alpha - t) + \sin(\alpha - t)\,(\cos(\alpha - t) - 4)\big)\Big),\\
B_2^5(t) &= \tfrac{2s_1}{3n_2}\Big(8\sin^3\big(\tfrac{\alpha - t}{2}\big)\,\sin\big(\tfrac{t}{2}\big) - \tfrac{n_0}{n_1}\sin^4\big(\tfrac{\alpha - t}{2}\big) + \tfrac{2s_1^4}{n_1}\big(3(\alpha - t) + \sin(\alpha - t)\,(\cos(\alpha - t) - 4)\big)\Big),\\
B_3^5(t) &= \tfrac{2s_1}{3n_2}\Big(8\sin^3\big(\tfrac{t}{2}\big)\,\sin\big(\tfrac{\alpha - t}{2}\big) - \tfrac{n_0}{n_1}\sin^4\big(\tfrac{t}{2}\big) + \tfrac{2s_1^4}{n_1}\big(3t + \sin(t)\,(\cos(t) - 4)\big)\Big),\\
B_4^5(t) &= \tfrac{4s_1}{n_0 n_1}\Big(n_0 \sin^4\big(\tfrac{t}{2}\big) - 2s_1^4\big(3t + \sin(t)\,(\cos(t) - 4)\big)\Big),\\
B_5^5(t) &= \tfrac{2}{n_0}\Big(3t + \sin(t)\,(\cos(t) - 4)\Big).
\end{aligned} \tag{6}$$

As in the previous case, the parameter α plays a tension-like effect which is illustrated in Figure 3(a)-(c). Moreover, when α tends to 2π the normalized B-basis in (6) assumes the following form

$$\begin{aligned}
&\lim_{\alpha\to 2\pi} B_0^5(t) = \frac{1}{12\pi}\,(12\pi - 6t + 8\sin(t) - \sin(2t)),\\
&\lim_{\alpha\to 2\pi} B_1^5(t) = \lim_{\alpha\to 2\pi} B_2^5(t) = \lim_{\alpha\to 2\pi} B_3^5(t) = \lim_{\alpha\to 2\pi} B_4^5(t) = 0,\\
&\lim_{\alpha\to 2\pi} B_5^5(t) = \frac{1}{12\pi}\,(6t - 8\sin(t) + \sin(2t)).
\end{aligned}$$

This limit case is illustrated in Figure 3(d).

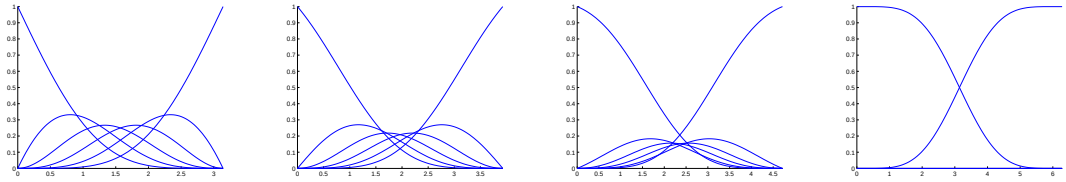

(a) (b) (c) (d)

Fig. 3 Basis functions $B_i^5(t)$, $i = 0, ..., 5$ for $t \in [0, \alpha]$ and $\alpha = \pi$ (a), $\alpha = \frac{5}{4}\pi$ (b), $\alpha = \frac{3}{2}\pi$ (c), $\alpha \to 2\pi$ (d).

In [14] it was also proven that the normalized B-basis $\{B_i^5(t)\}_{i=0,...,5}$ of the space U_5 tends to the ordinary Bernstein polynomials of degree 5 as α approaches 0. In addition, if the free parameter α is restricted to the interval $(0, \frac{2}{3}\pi)$, then the space U_5 is an extended Chebyshev space and the normalized B-basis $\{B_i^5(t)\}_{i=0,...,5}$ for such a space can be obtained using an iterative integral procedure starting from the (not normalized) B-basis $\{B_i^3(t)\}_{i=0,...,3}$ for the extended Chebyshev space $U_3 := \langle \sin(t), \cos(t), \sin(2t), \cos(2t) \rangle$ where $t \in [0, \alpha]$ and $0 < \alpha < \frac{2}{3}\pi$ (see [16]).

3 AT-Bézier curves over the mixed algebraic-trigonometric space U_5

In the following we refer to the parametric curves defined over the mixed algebraic-trigonometric space U_5 as *Algebraic-Trigonometric Bézier curves* or *AT-Bézier curves*. From the results in [14] it is well known that, since the space U_5 has a normalized B-basis, then we can define parametric curves over U_5 through a control polygon in a similar way to our familiar polynomial Bézier case. More precisely, an AT-Bézier curve defined over the space U_5 can be described by the Bézier-like form

$$\mathbf{x}(t) = \sum_{i=0}^{5} \mathbf{p}_i \, B_i^5(t) \,, \qquad t \in [0, \alpha], \quad 0 < \alpha < 2\pi, \tag{7}$$

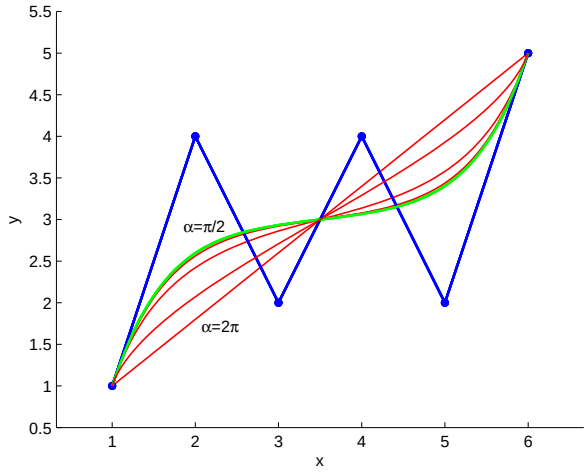

Fig. 4 Comparison of an ordinary degree 5 Bézier curve (thicker/green line) and AT–Bézier curves (thin/red lines) for $\alpha = \frac{\pi}{2}, \pi, \frac{3}{2}\pi, 2\pi$ obtained from the same control polygon (blue).

where B_i^5, $i = 0, \cdots, 5$ are the basis functions given in (6). These curves possess all the good properties of polynomial Bézier curves such as containment in the convex hull, affine invariance, variation

diminishing, interpolation of end points and tangency to the control polygon at the end points [1]. Furthermore they depend on the parameter α which can be used as shape parameter. Figure 4 shows the ordinary degree 5 Bézier curve compared to AT–Bézier curves obtained for different values of α, starting from the same control polygon. As mentioned in the previous section, for $\alpha \to 0$ the quintic polynomial Bézier curve is recovered, and for $\alpha \to 2\pi$ the straight line segment through $\mathbf{p}_0$ and $\mathbf{p}_5$ is obtained. Another interesting feature of AT–Bézier curves is their capability of reproducing arcs of arbitrary length (depending on the choice of $\alpha \in (0, 2\pi)$) of planar trigonometric curves in U_5, such as the ones displayed in Figure 5.

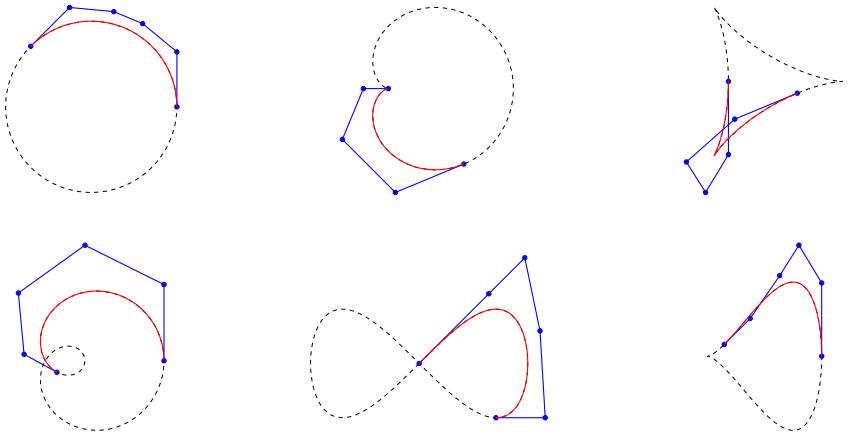

Fig. 5 Reproduction of arcs of different trigonometric curves by means of AT–Bézier curves over U_5 with $\alpha = \frac{3}{4}\pi$. From left to right, circle, cardioid, deltoid (top), limacon, lemniscate, piriform (bottom).

To the best of our knowledge a de Casteljau-like algorithm providing a stable and exact evaluation of AT-Bézier curves defined over the mixed algebraic-trigonometric space U_5 has never been proposed in the literature. In this section, we derive this kind of corner cutting algorithm, supported by the results in [13]. To this end, we start by observing that the basis functions $\{B_i^5\}_{i=0,\dots,5}$ of the space U_5 verify the following recurrence relation in terms of the basis functions $\{\tilde{B}_i^4\}_{i=0,\dots,4}$ of the space $\tilde{U}_4$:

$$B_i^5(t) = \lambda_{i-1}^4(t)\,\tilde{B}_{i-1}^4(t) + (1 - \lambda_i^4(t))\,\tilde{B}_i^4(t), \qquad i = 0, \dots, 5 \tag{8}$$

where

$$\begin{aligned}
\lambda_{-1}^4(t) &= \lambda_5^4(t) \equiv 0,\\
\lambda_0^4(t) &= \frac{n_0 \sin^4(\frac{\alpha-t}{2}) - 2s_1^4\left(3(\alpha-t)+\sin(\alpha-t)(\cos(\alpha-t)-4)\right)}{n_0 \sin^4(\frac{\alpha-t}{2})},\\
\lambda_1^4(t) &= \frac{2s_1^4\left(3(\alpha-t)+\sin(\alpha-t)(\cos(\alpha-t)-4)\right) - n_0 \sin^4(\frac{\alpha-t}{2}) + 8n_1 \sin^3(\frac{\alpha-t}{2})\sin(\frac{t}{2})}{8n_1 \sin^3(\frac{\alpha-t}{2})\sin(\frac{t}{2})},\\
\lambda_2^4(t) &= \frac{2s_1^4\left(3t+\sin(t)(\cos(t)-4)\right) - n_0 \sin^4(\frac{t}{2}) + 8n_1 \sin^3(\frac{t}{2})\sin(\frac{\alpha-t}{2})}{12n_2 \sin^2(\frac{t}{2})\sin^2(\frac{\alpha-t}{2})},\\
\lambda_3^4(t) &= \frac{n_0 \sin^4(\frac{t}{2}) - 2s_1^4\left(3t+\sin(t)(\cos(t)-4)\right)}{8n_1 \sin^3(\frac{t}{2})\sin(\frac{\alpha-t}{2})},\\
\lambda_4^4(t) &= \frac{2s_1^4\left(3t+\sin(t)(\cos(t)-4)\right)}{n_0 \sin^4(\frac{t}{2})},
\end{aligned} \tag{9}$$

with s_1 in (4) and n_0, n_1, n_2 the abbreviations in (5).

For all α in $(0, 2\pi)$ the functions $\lambda_i^4(t)$, $i = 0, \dots, 4$ defined in (9) satisfy the following properties:

(a) $\lambda_i^4 : [0, \alpha] \to [0, 1]$;
(b) $\lambda_i^4(0) = 0$ and $\lambda_i^4(\alpha) = 1$;
(c) λ_i^4 is monotonically increasing;
(d) $\lambda_i^4(t) = 1 - \lambda_{4-i}^4(\alpha - t)$.

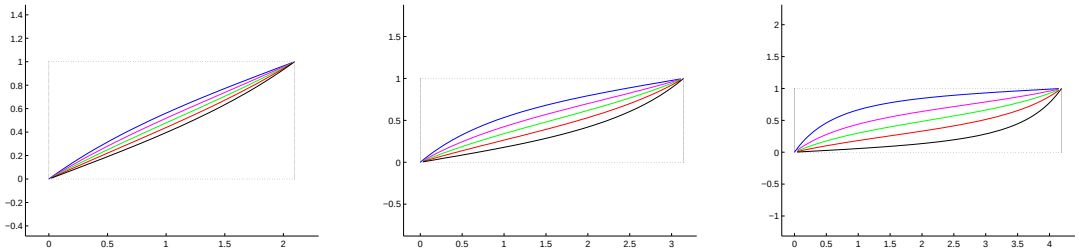

(a) (b) (c)

Fig. 6 Illustration of the functions $\lambda_i^4(t)$, $i = 0, ..., 4$ (appearing from top to bottom) for $t \in [0, \alpha]$ and $\alpha = \frac{2}{3}\pi$ (a), $\alpha = \pi$ (b), $\alpha = \frac{4}{3}\pi$ (c).

Figure 6 shows different sets of functions $\{\lambda_i^4(t)\}_{i=0,...,4}$ corresponding to different choices of α. Thus, in view of (8), we can write

$$\mathbf{x}(t) = \sum_{i=0}^{5} \mathbf{p}_i^0 \, B_i^5(t) = \sum_{i=0}^{4} \mathbf{p}_i^1 \, \tilde{B}_i^4(t)$$

with

$$\mathbf{p}_i^1 = (1 - \lambda_i^4(t)) \, \mathbf{p}_i^0 + \lambda_i^4(t) \, \mathbf{p}_{i+1}^0, \qquad i = 0, ..., 4. \tag{10}$$

Then, we proceed by defining the vector $\boldsymbol{\mu}^0 := [1, \cos(\frac{\alpha}{2}), \frac{1}{3}(1+2\cos^2(\frac{\alpha}{2})), \cos(\frac{\alpha}{2}), 1]$ whose i-th entry is given by equation (1) with $m = 4$. Exploiting the results in [13] where a de Casteljau-like algorithm (also called B-algorithm) for trigonometric curves defined over the space $\tilde{U}_4$ is proposed, we complete the last 4 steps of the corner cutting algorithm for evaluating AT-Bézier curves in U_5 as follows:

$$\begin{aligned}
&\text{for } i = 0 : 3 \\
&\quad \text{for } j = 0 : 3 - i \\
&\qquad \boldsymbol{\mu}_j^{i+1} = \sin(\tfrac{\alpha - t}{2}) \boldsymbol{\mu}_j^i + \sin(\tfrac{t}{2}) \boldsymbol{\mu}_{j+1}^i; \\
&\qquad \mathbf{p}_j^{i+2} = \sin(\tfrac{\alpha - t}{2}) \frac{\boldsymbol{\mu}_j^i}{\boldsymbol{\mu}_j^{i+1}} \mathbf{p}_j^{i+1} + \sin(\tfrac{t}{2}) \frac{\boldsymbol{\mu}_{j+1}^i}{\boldsymbol{\mu}_j^{i+1}} \mathbf{p}_{j+1}^{i+1}; \\
&\quad \text{end} \\
&\text{end}
\end{aligned} \tag{11}$$

There follows that $\mathbf{x}(t) = \mathbf{p}_0^5$ for any arbitrary $t \in [0, \alpha]$. In Figure 7 we illustrate the 5 steps of the de Casteljau-like algorithm given by (10)-(11) for the evaluation of AT-Bézier curves in U_5.

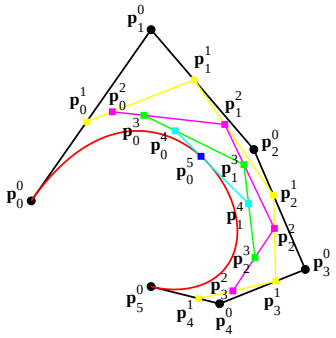

Fig. 7 The corner cutting scheme corresponding to the de Casteljau-like algorithm for the evaluation of an AT-Bézier curve defined over U_5 with $\alpha = \frac{2}{3}\pi$, at the parameter $t = \frac{\pi}{4} \in [0, \alpha]$.

4 Algebraic-Trigonometric Pythagorean Hodograph (ATPH) curves and their properties

Exploiting the fact that if $f \in \tilde{U}_2$ then $f^2 \in \tilde{U}_4$ and $\int f^2 \in U_5$, we now extend the well–known definition of polynomial Pythagorean–Hodograph (PH) curves [3] to the algebraic-trigonometric case, replacing the space of quadratic polynomials $\langle 1, t, t^2\rangle$ by the space $\tilde{U}_2 = \langle 1, \sin(t), \cos(t)\rangle$. Since $f \in \tilde{U}_2$ is defined for $\alpha \in (0, \pi)$, the construction of the new class of Pythagorean-Hodograph curves is restricted to $t \in [0, \alpha]$ with $\alpha \in (0, \pi)$.

Definition 1 Let $u(t)$, $v(t)$ and $\zeta(t)$ be non-zero real functions in the space $\tilde{U}_2$ such that $u(t)$ and $v(t)$ are relatively prime (namely $\gcd(u(t), v(t)) = 1$)[1] and both non–constant. Then, a planar parametric curve $\mathbf{x}(t) = (x(t),\, y(t))$ whose first derivative is of the form

$$x'(t) = \zeta(t)\Big(u^2(t) - v^2(t)\Big) \qquad \text{and} \qquad y'(t) = 2\zeta(t)u(t)v(t) \tag{12}$$

is called *Algebraic–Trigonometric PH curve* or *ATPH curve*.

As in the case of polynomial PH curves [3, 5], the curve's parametric speed is given by

$$\sigma(t) := \sqrt{(x'(t))^2 + (y'(t))^2} = \zeta(t)\,(u^2(t) + v^2(t)) \tag{13}$$

and its unit tangent, unit normal and (signed) curvature are given respectively by

$$\mathbf{t} = \frac{(u^2 - v^2, 2uv)}{u^2 + v^2}, \quad \mathbf{n} = \frac{(2uv, v^2 - u^2)}{u^2 + v^2}, \quad \kappa = \frac{2(uv' - u'v)}{\zeta(u^2 + v^2)^2}, \tag{14}$$

where, for conciseness, in (14) the parameter t is omitted.
In the following we will restrict our attention to the regular case $\zeta(t) = 1$. In this case the representation (12) may be obtained by squaring the complex function $\mathbf{w}(t) = u(t) + \mathrm{i}v(t)$ yielding $\mathbf{w}^2(t) = u^2(t) - v^2(t) + \mathrm{i}2u(t)v(t)$. The hodograph (12) is thus given by the real and imaginary part of $\mathbf{w}^2(t)$. In the remainder of the paper we will exclusively use this complex notation, and we thus write

$$\mathbf{x}'(t) = x'(t) + \mathrm{i}y'(t) = u^2(t) - v^2(t) + \mathrm{i}2u(t)v(t) = \mathbf{w}^2(t)\,, \tag{15}$$

as also previously done for planar PH quintics [3, 5]. Since here $\mathbf{w}(t)$ is a complex function in the space $\tilde{U}_2$ we write

$$\mathbf{w}(t) = \mathbf{w}_0\tilde{B}_0^2(t) + \mathbf{w}_1\tilde{B}_1^2(t) + \mathbf{w}_2\tilde{B}_2^2(t)\,, \tag{16}$$

where $\mathbf{w}_j \in \mathbb{C}$ for $j = 0, 1, 2$. By integrating (15) we obtain a parametric curve in the mixed algebraic-trigonometric space U_5 which can be expressed in the normalized B-basis (6), as formulated in the following proposition which results a generalization of [5, Proposition 1].

Proposition 1 *A planar, parametric curve over the mixed algebraic–trigonometric space U_5 expressed in terms of the normalized B-basis (6) as*

$$\mathbf{x}(t) = \sum_{i=0}^{5} \mathbf{p}_i B_i^5(t), \qquad t \in [0, \alpha], \tag{17}$$

is a (non-cuspidal) Algebraic–Trigonometric PH curve in the sense of Definition 1 if and only if its control points can be expressed in the form

$$\mathbf{p}_1 = \mathbf{p}_0 + \frac{n_0}{16s_1^4}\mathbf{w}_0^2, \tag{18}$$

$$\mathbf{p}_2 = \mathbf{p}_1 + \frac{n_0 - 6n_2}{8s_1^4}\mathbf{w}_0\mathbf{w}_1, \tag{19}$$

$$\mathbf{p}_3 = \mathbf{p}_2 + \frac{n_2}{4s_1^4}\Big((1 + c_2)\mathbf{w}_1^2 + \mathbf{w}_0\mathbf{w}_2\Big), \tag{20}$$

$$\mathbf{p}_4 = \mathbf{p}_3 + \frac{n_0 - 6n_2}{8s_1^4}\mathbf{w}_1\mathbf{w}_2, \tag{21}$$

$$\mathbf{p}_5 = \mathbf{p}_4 + \frac{n_0}{16s_1^4}\mathbf{w}_2^2, \tag{22}$$

where $\mathbf{w}_0, \mathbf{w}_1, \mathbf{w}_2$ are complex values and s_1, c_2, n_0, n_2 denote the abbreviations in (4)-(5).

[1] The greatest common divisor (gcd) here is the gcd of the bivariate polynomials (see e.g. [18]) $u(t) := u(\xi_1, \xi_2)$, $v(t) := v(\xi_1, \xi_2)$ where $\xi_1 = \sin(t)$, $\xi_2 = \cos(t)$.

Proof We substitute the function (16) into (15) and by integrating we obtain

$$\mathbf{x}(t) = \int \mathbf{x}'(t)\,dt = \mathbf{k} + \mathbf{a}_0 + \mathbf{a}_1 t + \mathbf{a}_2 \sin(t) + \mathbf{a}_3 \cos(t) + \mathbf{a}_4 \sin(2t) + \mathbf{a}_0 \cos(2t) \tag{23}$$

where

$$\mathbf{a}_0 = -\frac{1}{2}\mathbf{u}_1\mathbf{u}_2\,, \quad \mathbf{a}_1 = \frac{1}{2}(\mathbf{u}_1^2 + \mathbf{u}_2^2) + \mathbf{u}_0^2\,, \quad \mathbf{a}_2 = 2\mathbf{u}_0\mathbf{u}_2\,, \quad \mathbf{a}_3 = -2\mathbf{u}_0\mathbf{u}_1\,, \quad \mathbf{a}_4 = \frac{1}{4}(-\mathbf{u}_1^2 + \mathbf{u}_2^2),$$

with

$$\mathbf{u}_0 = \frac{(1+c_2)\mathbf{w}_1 - \mathbf{w}_0 - \mathbf{w}_2}{c_2 - 1}\,, \quad \mathbf{u}_1 = \frac{s_2(\mathbf{w}_0 - \mathbf{w}_1)}{c_2 - 1}\,, \quad \mathbf{u}_2 = \frac{c_2(\mathbf{w}_0 - \mathbf{w}_1) + \mathbf{w}_2 - \mathbf{w}_1}{c_2 - 1} \tag{24}$$

and $\mathbf{k}$ the integration constant. Expressing the basis functions of the functional space U_5 in terms of the normalized B–basis (6) and substituting these basis functions in (23) yields the expressions (18)-(22), where $\mathbf{p}_0 = \mathbf{k} - \frac{c_1}{2s_1^3}\,(\mathbf{w}_0 - \mathbf{w}_1)\,(c_2(\mathbf{w}_0 + \mathbf{w}_1) + \mathbf{w}_1 - 2\mathbf{w}_0 - \mathbf{w}_2)$. □

By (13) we have $\sigma(t) := \sqrt{(x'(t))^2 + (y'(t))^2} = |\mathbf{w}^2(t)|$, and thus the arc-length of an ATPH curve is explicitly given by

$$\int \sigma(t)dt = \tfrac{1}{2}\left(-\gamma_{12} + (2\gamma_{00} + \gamma_{11} + \gamma_{22})t + 4\gamma_{02}\sin(t) - 4\gamma_{01}\cos(t) + \tfrac{1}{2}(\gamma_{22} - \gamma_{11})\sin(2t) - \gamma_{12}\cos(2t)\right), \tag{25}$$

where

$$\gamma_{ij} = \mathrm{Re}\left(\frac{\mathbf{u}_i}{\mathbf{u}_j}\right)|\mathbf{u}_j|^2, \qquad i,j \in \{0,1,2\}, \tag{26}$$

with $\mathbf{u}_i$, $i = 0,1,2$ in (24). We continue by showing that, like polynomial PH curves, ATPH curves admit not only an exact representation of the arc-length, but also of their offset curves. In the following, the offset curve of the ATPH curve $\mathbf{x}(t) = \sum_{i=0}^{5} \mathbf{p}_i B_i^5(t)$, $t \in [0,\alpha]$ at oriented distance d along the unit normal vector $\mathbf{n}(t)$ is denoted by $\mathbf{x}_d(t)$ and given by $\mathbf{x}_d(t) = \mathbf{x}(t) + d\,\mathbf{n}(t)$, $t \in [0,\alpha]$. The normal vector $\mathbf{n}$ has a rational ATPH representation over the space $\tilde{U}_4 = \langle 1, \sin(t), \cos(t), \sin(2t), \cos(2t)\rangle$ since

$$\mathbf{n}(t) = \frac{-\mathrm{i}\mathbf{w}^2(t)}{\mathbf{w}(t)\overline{\mathbf{w}}(t)}\,,$$

where

$$\mathbf{w}^2(t) = \mathbf{w}_0^2\tilde{B}_0^4(t) + \mathbf{w}_0\mathbf{w}_1\tilde{B}_1^4(t) + \frac{\mathbf{w}_0\mathbf{w}_2 + (1+\cos(\alpha))\mathbf{w}_1^2}{2+\cos(\alpha)}\,\tilde{B}_2^4(t) + \mathbf{w}_1\mathbf{w}_2\tilde{B}_3^4(t) + \mathbf{w}_2^2\tilde{B}_4^4(t), \tag{27}$$

and

$$\begin{aligned}\mathbf{w}(t)\overline{\mathbf{w}}(t) = {} & \mathbf{w}_0\overline{\mathbf{w}}_0\tilde{B}_0^4(t) + \tfrac{1}{2}(\mathbf{w}_0\overline{\mathbf{w}}_1 + \mathbf{w}_1\overline{\mathbf{w}}_0)\tilde{B}_1^4(t) + \tfrac{\mathbf{w}_0\overline{\mathbf{w}}_2 + 2(1+\cos(\alpha))\mathbf{w}_1\overline{\mathbf{w}}_1 + \mathbf{w}_2\overline{\mathbf{w}}_0}{2(2+\cos(\alpha))}\,\tilde{B}_2^4(t) \\ & + \tfrac{1}{2}(\mathbf{w}_1\overline{\mathbf{w}}_2 + \mathbf{w}_2\overline{\mathbf{w}}_1)\tilde{B}_3^4(t) + \mathbf{w}_2\overline{\mathbf{w}}_2\tilde{B}_4^4(t)\,,\end{aligned}$$

with $\tilde{B}_i^4(t)$, $i = 0,\ldots,4$ from (2). We thus obtain

$$\mathbf{n}(t) = \frac{\displaystyle\sum_{i=0}^{4} \tilde{v}_i\tilde{\mathbf{p}}_i\,\tilde{B}_i^4(t)}{\displaystyle\sum_{j=0}^{4} \tilde{v}_j\,\tilde{B}_j^4(t)}, \qquad t \in [0,\alpha],$$

where

$$\begin{aligned}
&\tilde{v}_0 = \mathbf{w}_0\overline{\mathbf{w}}_0 = |\mathbf{w}_0|^2, && \tilde{v}_0\tilde{\mathbf{p}}_0 = -\mathrm{i}\mathbf{w}_0^2,\\
&\tilde{v}_1 = \tfrac{1}{2}(\mathbf{w}_0\overline{\mathbf{w}}_1 + \mathbf{w}_1\overline{\mathbf{w}}_0), && \tilde{v}_1\tilde{\mathbf{p}}_1 = -\mathrm{i}\mathbf{w}_0\mathbf{w}_1,\\
&\tilde{v}_2 = \tfrac{\mathbf{w}_0\overline{\mathbf{w}}_2 + 2(1+\cos(\alpha))\mathbf{w}_1\overline{\mathbf{w}}_1 + \mathbf{w}_2\overline{\mathbf{w}}_0}{2(2+\cos(\alpha))}, && \tilde{v}_2\tilde{\mathbf{p}}_2 = -\mathrm{i}\,\tfrac{\mathbf{w}_0\mathbf{w}_2 + (1+\cos(\alpha))\mathbf{w}_1^2}{2+\cos(\alpha)},\\
&\tilde{v}_3 = \tfrac{1}{2}(\mathbf{w}_1\overline{\mathbf{w}}_2 + \mathbf{w}_2\overline{\mathbf{w}}_1), && \tilde{v}_3\tilde{\mathbf{p}}_3 = -\mathrm{i}\mathbf{w}_1\mathbf{w}_2,\\
&\tilde{v}_4 = \mathbf{w}_2\overline{\mathbf{w}}_2 = |\mathbf{w}_2|^2, && \tilde{v}_4\tilde{\mathbf{p}}_4 = -\mathrm{i}\mathbf{w}_2^2.
\end{aligned}$$

Now, since $\mathbf{x}(t) = \sum_{i=0}^{5} \mathbf{p}_i B_i^5(t)$, we can define the offset curve $\mathbf{x}_d(t)$ as a rational algebraic-trigonometric curve in terms of the normalized B-basis of the function space obtained from the multiplication of $\tilde{U}_4$ and U_5. Recall that being $\tilde{U}_2 = \langle 1, \sin(t), \cos(t)\rangle$, $\tilde{U}_4 = \langle 1, \sin(t), \cos(t), \sin(2t), \cos(2t)\rangle$ and $\tilde{U}_8 = \langle 1, \sin(t), \cos(t), \sin(2t), \cos(2t), \sin(3t), \cos(3t), \sin(4t), \cos(4t)\rangle$, then the relationships $\tilde{U}_2 * \tilde{U}_2 = \tilde{U}_4$ and $\tilde{U}_4 * \tilde{U}_4 = \tilde{U}_8$ are satisfied, with $*$ denoting the product between the two function spaces. Therefore, being $U_5 = \langle 1, t, \sin(t), \cos(t), \sin(2t), \cos(2t)\rangle$ we have

$$\hat{U} := \tilde{U}_4 * U_5 = \langle \tilde{U}_8, t, t\sin(t), t\cos(t), t\sin(2t), t\cos(2t)\rangle.$$

The offset curve $\mathbf{x}_d(t)$ of the ATPH curve $\mathbf{x}(t)$ is thus a rational algebraic-trigonometric curve of the form

$$\mathbf{x}_d(t) = \mathbf{x}(t) + d\,\mathbf{n}(t) = \sum_{i=0}^{5} \mathbf{p}_i B_i^5(t) \,+\, d\,\frac{\displaystyle\sum_{i=0}^{4} \tilde{v}_i \tilde{\mathbf{p}}_i\, \tilde{B}_i^4(t)}{\displaystyle\sum_{j=0}^{4} \tilde{v}_j\, \tilde{B}_j^4(t)} = \frac{\displaystyle\sum_{i=0}^{13} \hat{v}_i\, \hat{\mathbf{p}}_i\, \hat{B}_i^{13}(t)}{\displaystyle\sum_{j=0}^{13} \hat{v}_j \hat{B}_j^{13}(t)}, \qquad t \in [0, \alpha],$$

where $\hat{B}_i^{13}$, $i = 0, ..., 13$ are the basis functions of the space $\hat{U}$. This normalized B–basis of $\hat{U}$ will be presented in a forthcoming article. Note that, while the PH quintic has a rational offset of order 10 (see [9]), for the analogous ATPH curve the offset representation requires a basis of order 14.

5 C^1 Hermite interpolation problem

In this section we extend the solution to the following problem, as presented for polynomial PH curves in [5], to the context of ATPH curves.

Problem 1. Given arbitrary control points $\mathbf{p}_0 \neq \mathbf{p}_1$ and $\mathbf{p}_4 \neq \mathbf{p}_5$ of an AT-Bézier curve $\mathbf{x}(t) = \sum_{i=0}^{5} \mathbf{p}_i B_i^5(t)$, $t \in [0, \alpha]$, defined over the space U_5, we look for the two remaining inner control points $\mathbf{p}_2$ and $\mathbf{p}_3$ such that all six are expressible in the form given by equations (18)-(22) for some complex values $\mathbf{w}_0$,$\mathbf{w}_1$,$\mathbf{w}_2$. Since AT-Bézier curves built-upon the normalized B-basis B_i^5, $i = 0, \cdots, 5$ satisfy

$$\mathbf{x}(0) = \mathbf{p}_0, \quad \mathbf{x}(\alpha) = \mathbf{p}_5, \quad \mathbf{x}'(0) = \frac{16 s_1^4}{n_0}(\mathbf{p}_1 - \mathbf{p}_0), \quad \mathbf{x}'(\alpha) = \frac{16 s_1^4}{n_0}(\mathbf{p}_5 - \mathbf{p}_4),$$

with s_1 in (4) and n_0 in (5), this problem can be obviously regarded as a C^1 Hermite interpolation problem to prescribed end points $\mathbf{p}_0$, $\mathbf{p}_5$ and tangent vectors at these end points. Hereinafter the tangent vectors at $\mathbf{p}_0$, $\mathbf{p}_5$ will be denoted by $\mathbf{d}_0, \mathbf{d}_2$, respectively, since (as we will see later) they are directly related to the values of $\mathbf{w}_0$,$\mathbf{w}_2$.

5.1 ATPH interpolants solving the C^1 Hermite problem

In order to solve *Problem* 1 we propose a variation of the method proposed in [5] to solve the Hermite interpolation problem by polynomial PH quintics.

Proposition 2 *The solutions of the Hermite interpolation Problem* 1 *in terms of the complex values* $\mathbf{w}_0, \mathbf{w}_1, \mathbf{w}_2$ *are given by*

$$\begin{aligned}
\mathbf{w}_0 &= \pm|\mathbf{d}_0|^{\frac{1}{2}} \exp\left(\mathrm{i}\frac{\omega_0}{2}\right) = \pm|\mathbf{d}_0|^{\frac{1}{2}} \left(\cos\left(\frac{\omega_0}{2}\right) + \mathrm{i}\sin\left(\frac{\omega_0}{2}\right)\right), \\
\mathbf{w}_2 &= \pm|\mathbf{d}_2|^{\frac{1}{2}} \exp\left(\mathrm{i}\frac{\omega_2}{2}\right) = \pm|\mathbf{d}_2|^{\frac{1}{2}} \left(\cos\left(\frac{\omega_2}{2}\right) + \mathrm{i}\sin\left(\frac{\omega_2}{2}\right)\right), \\
\mathbf{w}_1 &= \pm|\mathbf{d}_1|^{\frac{1}{2}} \left(\cos\left(\frac{\omega_1}{2}\right) + \mathrm{i}\sin\left(\frac{\omega_1}{2}\right)\right) - \frac{n_0 - 6n_2}{4n_2(1+c_2)}(\mathbf{w}_0 + \mathbf{w}_2),
\end{aligned} \tag{28}$$

where

$$\begin{aligned}
\mathbf{d}_0 &= \tfrac{16 s_1^4}{n_0}(\mathbf{p}_1 - \mathbf{p}_0), \qquad \mathbf{d}_2 = \tfrac{16 s_1^4}{n_0}(\mathbf{p}_5 - \mathbf{p}_4), \\
\mathbf{d}_1 &= \tfrac{1}{1+c_2}\left(\tfrac{4 s_1^4}{n_2}(\mathbf{p}_4 - \mathbf{p}_1) + \tfrac{(n_0 - 6n_2)^2}{16 n_2^2 (1+c_2)}(\mathbf{w}_0 + \mathbf{w}_2)^2 - \mathbf{w}_0 \mathbf{w}_2\right),
\end{aligned}$$

$\omega_k = \arg(\mathbf{d}_k)$, $k = 0, 1, 2$ *and* s_1, c_2, n_0, n_2 *are the abbreviations in (4)-(5).*

Proof By de Moivre's theorem, from (18) and (22) we obtain the expressions of $\mathbf{w}_0$ and $\mathbf{w}_2$ in (28). Then, writing $\mathbf{p}_4 - \mathbf{p}_1 = (\mathbf{p}_4 - \mathbf{p}_3) + (\mathbf{p}_3 - \mathbf{p}_2) + (\mathbf{p}_2 - \mathbf{p}_1)$ and substituting from (18)-(22) we obtain

$$\frac{8s_1^4}{n_0 - 6n_2}(\mathbf{p}_4 - \mathbf{p}_1) = \mathbf{w}_1\mathbf{w}_2 + \frac{2n_2}{n_0 - 6n_2}((1 + c_2)\mathbf{w}_1^2 + \mathbf{w}_0\mathbf{w}_2) + \mathbf{w}_0\mathbf{w}_1. \tag{29}$$

By the change of variable

$$\widetilde{\mathbf{w}}_1 = \mathbf{w}_1 + \frac{n_0 - 6n_2}{4n_2(1 + c_2)}(\mathbf{w}_0 + \mathbf{w}_2), \tag{30}$$

equation (29) becomes

$$\widetilde{\mathbf{w}}_1^2 = \frac{4s_1^4}{n_2(1 + c_2)}(\mathbf{p}_4 - \mathbf{p}_1) + \frac{(n_0 - 6n_2)^2}{16n_2^2(1 + c_2)^2}(\mathbf{w}_0 + \mathbf{w}_2)^2 - \frac{1}{1 + c_2}\mathbf{w}_0\mathbf{w}_2\,. \tag{31}$$

From (31) we find

$$\widetilde{\mathbf{w}}_1 = \pm|\mathbf{d}_1|^{\frac{1}{2}} \exp\left(\mathrm{i}\frac{\omega_1}{2}\right) = \pm|\mathbf{d}_1|^{\frac{1}{2}} \left(\cos\left(\frac{\omega_1}{2}\right) + \mathrm{i}\sin\left(\frac{\omega_1}{2}\right)\right) \tag{32}$$

with

$$\mathbf{d}_1 = \frac{4s_1^4}{n_2(1 + c_2)}(\mathbf{p}_4 - \mathbf{p}_1) + \frac{(n_0 - 6n_2)^2}{16n_2^2(1 + c_2)^2}(\mathbf{w}_0 + \mathbf{w}_2)^2 - \frac{1}{1 + c_2}\mathbf{w}_0\mathbf{w}_2.$$

Finally, by substituting (32) in (30) the expression of $\mathbf{w}_1$ in (28) is obtained. □

Remark 1 As in the polynomial case (see [5, Remark 3]), in the expressions (28) we have three independent signs. Thus, we can construct eight ATPH interpolants. We remark that if we take (-$\mathbf{w}_0$, -$\mathbf{w}_1$, -$\mathbf{w}_2$) or ($\mathbf{w}_0$, $\mathbf{w}_1$, $\mathbf{w}_2$) the same interpolant is obtained. Moreover, we observe that in the expressions (18)-(22) we have homogeneous quadratic forms in the coefficients of $\mathbf{w}(t)$. As suggested in [5], we can thus fix the sign in any one of the three expressions (28) and obtain only four distinct interpolants.

Remark 2 We further observe that the free parameter α acts as a shape parameter for the ATPH interpolants. This can be clearly seen in Figure 8 where different ATPH interpolants to the same end points and associated end derivatives (all corresponding to a positive choice of the signs of $\mathbf{w}_0$ and $\mathbf{w}_2$) are displayed together with the standard polynomial PH quintic solving the same C^1 Hermite problem. In this figure, as well as in many other figures of this section, we refer to color lines to distinguish among multiple plots. We thus invite the reader to refer to the electronic version of the paper to make the identification of individual plots easier. We also note that, in Figure 8, for increasing values of α in $(0, \pi)$ the curves become longer and longer. This seems to be in contradiction to the behaviour of the AT-Bézier curves which, for increasing values of α in their range of definition, become shorter and shorter. The reason for this fact simply lies in the dependency on α of the control points of the ATPH curve according to equations (18)-(22).
Figure 9 shows the behaviour of all four possible families of ATPH curves interpolating the end points $\mathbf{p}_0 = 5\mathrm{i}$, $\mathbf{p}_5 = -3 - 4\mathrm{i}$ and the end derivatives $\mathbf{d}_0 = \mathbf{d}_2 = 25 - 15\mathrm{i}$, for different choices of $\alpha \in (0, \pi)$. We obtain the four families of ATPH interpolants from the sign choices $++$, $+-$, $-+$, $--$ in the expressions of $\mathbf{w}_0$ and $\mathbf{w}_2$. In the following we will always refer to the four families of ATPH interpolants by pointing out these sign combinations.
We conclude by observing that the arc-length of the ATPH curve (corresponding to the evaluation of the function in (25) between 0 and α) has the expression

$$\begin{aligned} S_\alpha = \int_0^\alpha \sigma(t)dt = {} & 2\gamma_{01} + \tfrac{1}{2}\gamma_{12} + (\gamma_{00} + \tfrac{1}{2}(\gamma_{11} + \gamma_{22}))\,\alpha + 2\gamma_{02}\sin(\alpha) - 2\gamma_{01}\cos(\alpha) \\ & + \tfrac{1}{4}(\gamma_{22} - \gamma_{11})\sin(2\alpha) - \tfrac{1}{2}\gamma_{12}\cos(2\alpha) \end{aligned} \tag{33}$$

with γ_{ij} in (26), and thus turns out to be monotonically increasing for increasing values of α, as clearly shown in Figure 10. Note that S_α is always a continuous function, but depending on the geometry of the family of curves it might not be differentiable for certain values of α, as can be seen in Figure 10 (bottom left) for the ATPH family appearing in Figure 8(b).
Inspired by the observation of numerous examples all exhibiting the same qualitative behaviour as the ones in Figures 8-9 and supported by the fact that, for $\alpha \in (0, \frac{2}{3}\pi)$, the algebraic-trigonometric space U_5 is an extended Chebyshev space (see [16]), hereinafter we will restrict the choice of α to the interval $(0, \frac{2}{3}\pi)$.

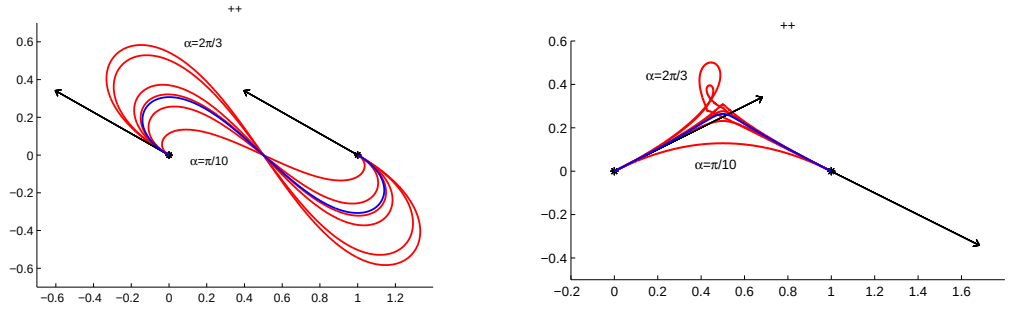

(a) $\mathbf{d}_0 = \mathbf{d}_2 = -3 + \mathrm{i}\frac{3(4+\sqrt{5})}{11}$ (b) $\mathbf{d}_0 = \frac{3(4+\sqrt{5})}{11}(2+\mathrm{i})$, $\mathbf{d}_2 = \frac{3(4+\sqrt{5})}{11}(2-\mathrm{i})$

Fig. 8 Comparison of ATPH interpolants (red curves) to the end points $\mathbf{p}_0 = 0$, $\mathbf{p}_5 = 1$ and associated end derivatives $\mathbf{d}_0$ and $\mathbf{d}_2$ (here plotted with a scale factor of $\frac{1}{5}$ to fit into the picture), obtained for a positive choice of $\mathbf{w}_0$ and $\mathbf{w}_2$ (++) and increasing values of $\alpha \in (0,\pi)$ (respectively $\alpha = \frac{\pi}{10}, \frac{\pi}{4}, \frac{\pi}{3}, \frac{2}{5}\pi, \frac{3}{5}\pi, \frac{2}{3}\pi$), with the (++) PH quintic interpolant (blue curve) solving the same C^1 Hermite interpolation problem.

5.2 How to identify the "best" ATPH Hermite interpolant

The *rotation index* $\mathcal{R}$ and the *absolute rotation index* $\mathcal{R}_{abs}$, respectively defined by

$$\mathcal{R} := \frac{1}{2\pi}\int_0^\alpha \kappa(t)|\mathbf{x}'(t)|dt\,, \qquad \mathcal{R}_{abs} := \frac{1}{2\pi}\int_0^\alpha |\kappa(t)||\mathbf{x}'(t)|dt\,,$$

are the quantities whose minimization allows us to identify the "best" ATPH Hermite interpolant [5]. Since $\kappa(t) = \frac{\mathrm{Im}(\bar{\mathbf{x}}'(t)\mathbf{x}''(t))}{|\mathbf{x}'(t)|^3}$, then $\kappa(t)|\mathbf{x}'(t)| = \frac{\mathrm{Im}(\bar{\mathbf{x}}'(t)\mathbf{x}''(t))}{|\mathbf{x}'(t)|^2}$ and in view of (15) $\kappa(t)|\mathbf{x}'(t)| = 2\mathrm{Im}\left(\frac{\mathbf{w}'(t)}{\mathbf{w}(t)}\right)$. The rotation and the absolute rotation indices can thus be rewritten in the equivalent form

$$\mathcal{R} = \frac{1}{2\pi\mathrm{i}}\int_0^\alpha \frac{\mathbf{w}'(t)\bar{\mathbf{w}}(t) - \mathbf{w}(t)\bar{\mathbf{w}}'(t)}{\mathbf{w}(t)\bar{\mathbf{w}}(t)}dt\,, \quad \mathcal{R}_{abs} = \frac{1}{2\pi}\int_0^\alpha \frac{|\mathbf{w}'(t)\bar{\mathbf{w}}(t) - \mathbf{w}(t)\bar{\mathbf{w}}'(t)|}{\mathbf{w}(t)\bar{\mathbf{w}}(t)}dt. \tag{34}$$

Recalling that $\mathbf{w}(t) = u(t) + \mathrm{i}v(t)$, we can also rewrite (34) in the real formulation as follows

$$\mathcal{R} = \frac{1}{\pi}\int_0^\alpha \frac{(u(t)v'(t) - u'(t)v(t))}{u(t)^2 + v(t)^2}dt\,, \quad \mathcal{R}_{abs} = \frac{1}{\pi}\int_0^\alpha \frac{|(u(t)v'(t) - u'(t)v(t))|}{u(t)^2 + v(t)^2}dt.$$

Now, if we define $z(t) := \frac{v(t)}{u(t)} \in \mathbb{R}$, we can apply [5, Lemma 3] thus obtaining

$$\begin{aligned}
\mathcal{R}^{ATPH} &= \tfrac{1}{\pi}\Big(\arctan(z(\alpha)) - \arctan(z(0))\Big) - \mathcal{I}_0^\alpha(z(t)),\\
\mathcal{R}^{ATPH}_{abs} &= \tfrac{1}{\pi}\left(\sum_{j=0}^{n-1}\mathrm{sign}_{I_j}(\xi(t))\Big(\arctan(z(t_{j+1})) - \arctan(z(t_j))\Big)\right) + \mathcal{S}(u(t))\,,
\end{aligned}$$

where

- $\mathcal{I}_0^\alpha(z(t))$ is the Cauchy index of $z(t)$;
- $\xi(t) = u(t)v'(t) - u'(t)v(t)$;
- t_j, $j = 0,\dots,n$ are the zeros of $\xi(t)$ in the interval $[0,\alpha]$ with $t_0 = 0$ and $t_n = \alpha$;
- $\mathrm{sign}_{I_j}(\xi(t))$ denotes the sign of $\xi(t)$ on the interval $I_j = [t_j, t_{j+1}]$, $j = 0,\dots,n-1$;
- $\mathcal{S}(u(t))$ is the number of zeros of $u(t)$ in the interval $[0,\alpha]$.

The examples in Figure 11 confirm how the "best" solution to the Hermite interpolation problem can be identified as the one with the smallest absolute rotation index (see Table 1). The purpose of Table 2 and Figure 12(a) is to show that ATPH interpolants compare favorably with their polynomial counterpart represented by the well-known PH quintics. In fact, for the chosen set of end points and associated end derivatives (taken from [12, Example 4]), we can see that all four possible PH curves

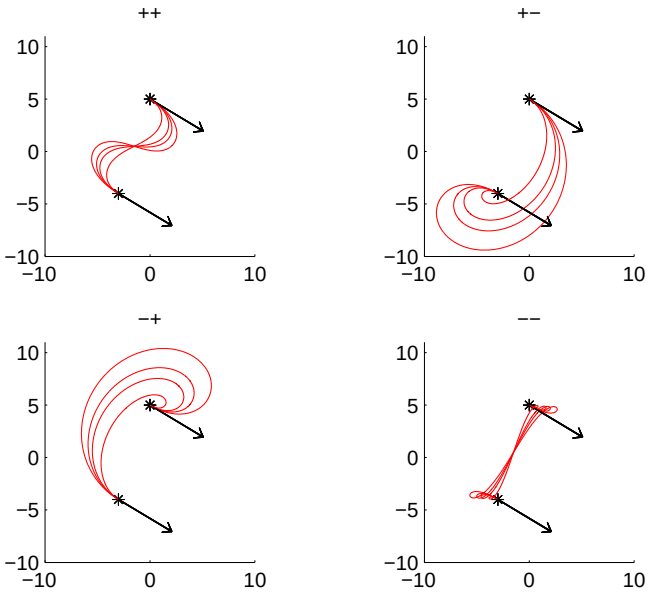

(a) $\alpha = \frac{\pi}{5}, \frac{\pi}{3}, \frac{2}{5}\pi, \frac{\pi}{2}$

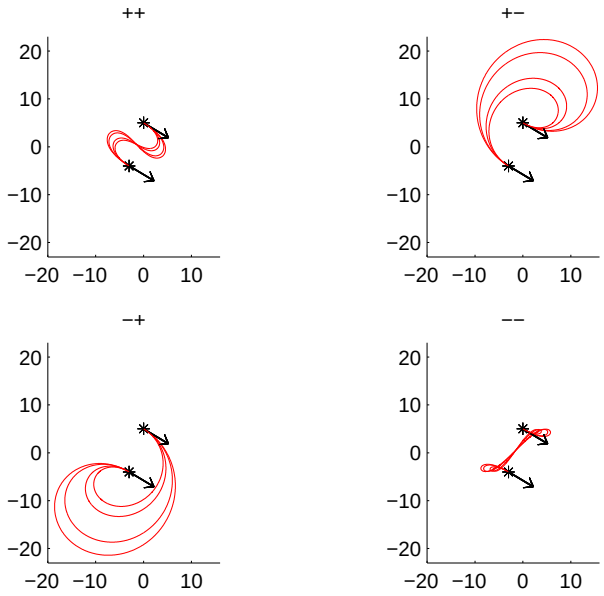

(b) $\alpha = \frac{7}{12}\pi, \frac{2}{3}\pi, \frac{5}{6}\pi, \frac{9}{10}\pi$

Fig. 9 The four families of ATPH interpolants to the end points $\mathbf{p}_0 = 5\mathrm{i}$, $\mathbf{p}_5 = -3 - 4\mathrm{i}$ and end derivatives $\mathbf{d}_0 = \mathbf{d}_2 = 25 - 15\mathrm{i}$ (here plotted with a scale factor of $\frac{1}{5}$), obtained for different values of $\alpha \in (0, \pi)$.

exhibit undesired self-intersections, although the standard cubic interpolant does not. For the same data, the (++) ATPH interpolant, e.g. for $\alpha = \frac{\pi}{5}$, not only lacks self-intersections (see Fig. 13(a)-(b)), but also has a more pleasant curvature behaviour than the standard cubic interpolant (see Fig. 13(c)). We conclude by observing that, for certain Hermite data, the concept of the "best" interpolant as the interpolant with the smallest absolute rotation index is ambiguous. An example of this phenomenon is represented in Figure 12(b) where we have two ATPH curves (the ones having signs (+−) and (−+)) with the same smallest absolute rotation index (see Table 3), none of them being optimal. In fact, the most similar to the standard cubic interpolant is still the one having signs (++).

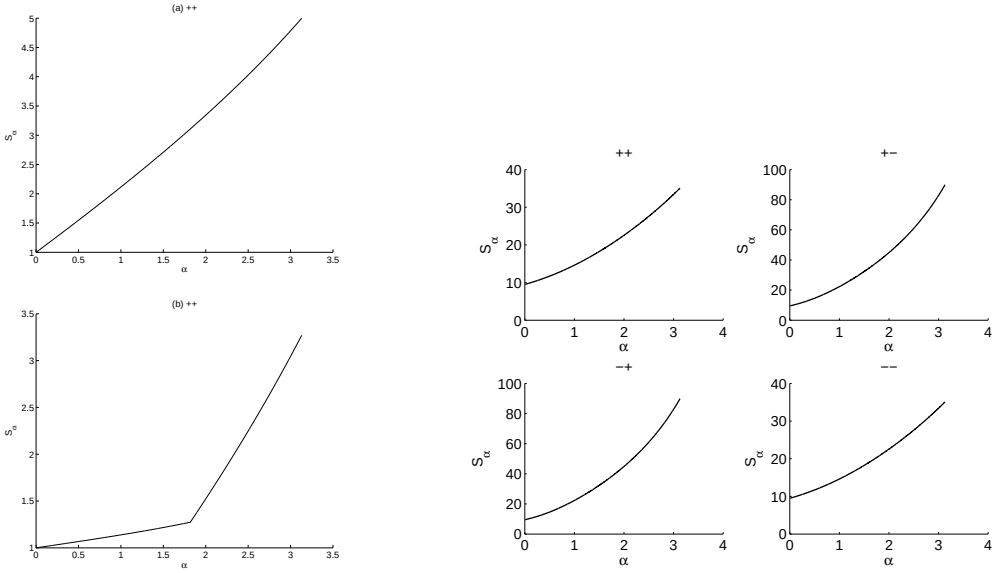

Fig. 10 Behaviour of the arc-length of the ATPH curves in Figure 8 (left) and in Figure 9 (right) for $\alpha \in (0, \pi)$.

R^{ATPH}_{abs}	(a)	(b)
(++)	0.8976	0.3589
(+−)	1.1515	0.7542
(−+)	1.1515	1.25
(−−)	1.024	1.75

Table 1 ATPH absolute rotation indices for the examples in Figure 11.

	R^{PH}_{abs}	R^{ATPH}_{abs}
(++)	1.395	0.7270
(+−)	1	1
(−+)	1	1
(−−)	1.5504	1.8959

Table 2 Comparison of PH and ATPH absolute rotation indices for the examples in Figure 12(a).

	R^{PH}_{abs}	R^{ATPH}_{abs}
(++)	1.1009	1.0831
(+−)	1	1
(−+)	1	1
(−−)	1.2266	1.2199

Table 3 Comparison of PH and ATPH absolute rotation indices for the examples in Figure 12(b).

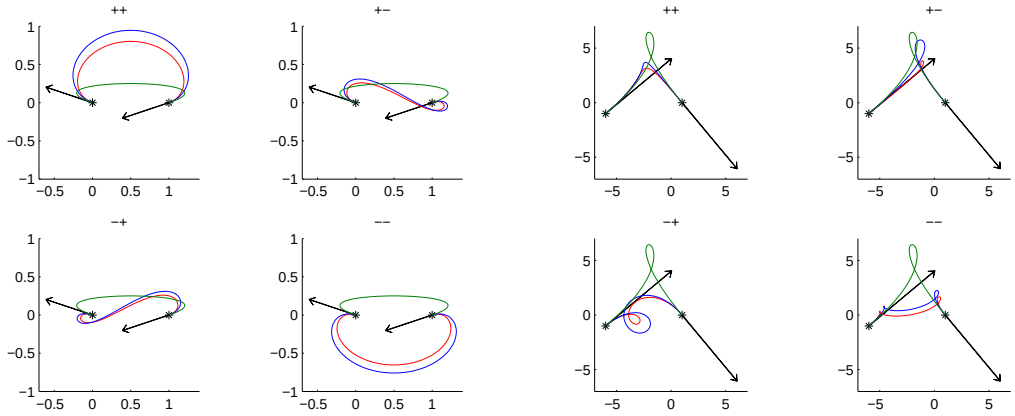

(a) $\mathbf{p}_0 = 0$, $\mathbf{p}_5 = 1$, $\mathbf{d}_0 = -3 + \mathrm{i}$, $\mathbf{d}_2 = -3 - \mathrm{i}$ (b) $\mathbf{p}_0 = -6 - \mathrm{i}$, $\mathbf{p}_5 = 1$, $\mathbf{d}_0 = 30 + 25\mathrm{i}$, $\mathbf{d}_2 = 25 - 30\mathrm{i}$

Fig. 11 Comparison of the ATPH interpolant obtained for $\alpha = \frac{\pi}{4}$ (red curve), with the corresponding PH quintic interpolant (blue curve) and the unique cubic interpolant (green curve) to the given end points $\mathbf{p}_0$,$\mathbf{p}_5$ and associated end derivatives $\mathbf{d}_0$,$\mathbf{d}_2$ (here plotted with a scale factor of $\frac{1}{5}$ to fit into the picture).

The criterion based on the absolute rotation index requires us to construct all four interpolants, and then compare a quantitative shape measure. In order to have the ability to construct directly the best interpolant only as the one being free of loops, we need to restrict our attention to cases with "reasonable" Hermite data. Adapting the reasoning in [12] to our non-polynomial context, in the remainder of this section we show that, given arbitrary end points $\mathbf{p}_0$ and $\mathbf{p}_5$, we can define "reasonable"

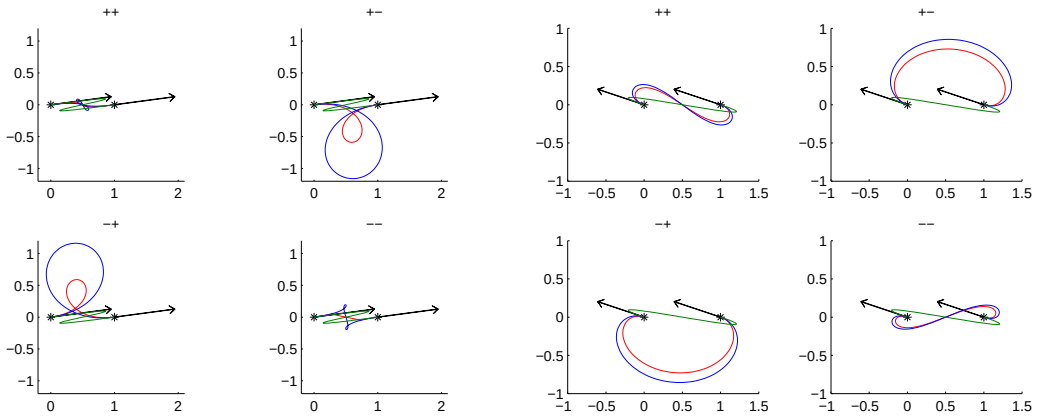

(a) $\mathbf{d}_0 = \mathbf{d}_2 = 7.5 + \mathrm{i}, \;\; \alpha = \frac{\pi}{5}$ (b) $\mathbf{d}_0 = \mathbf{d}_2 = -3 + \mathrm{i}, \;\; \alpha = \frac{\pi}{4}$

Fig. 12 The four ATPH interpolants (red curves) to the end points $\mathbf{p}_0 = 0$, $\mathbf{p}_5 = 1$ and associated end derivatives $\mathbf{d}_0, \mathbf{d}_2$ (plotted with a scale factor of $\frac{1}{8}$ in (a) and $\frac{1}{5}$ in (b)) obtained with the indicated value of α. The corresponding PH quintic interpolant and the unique cubic interpolant to the same data are drawn in blue and green, respectively.

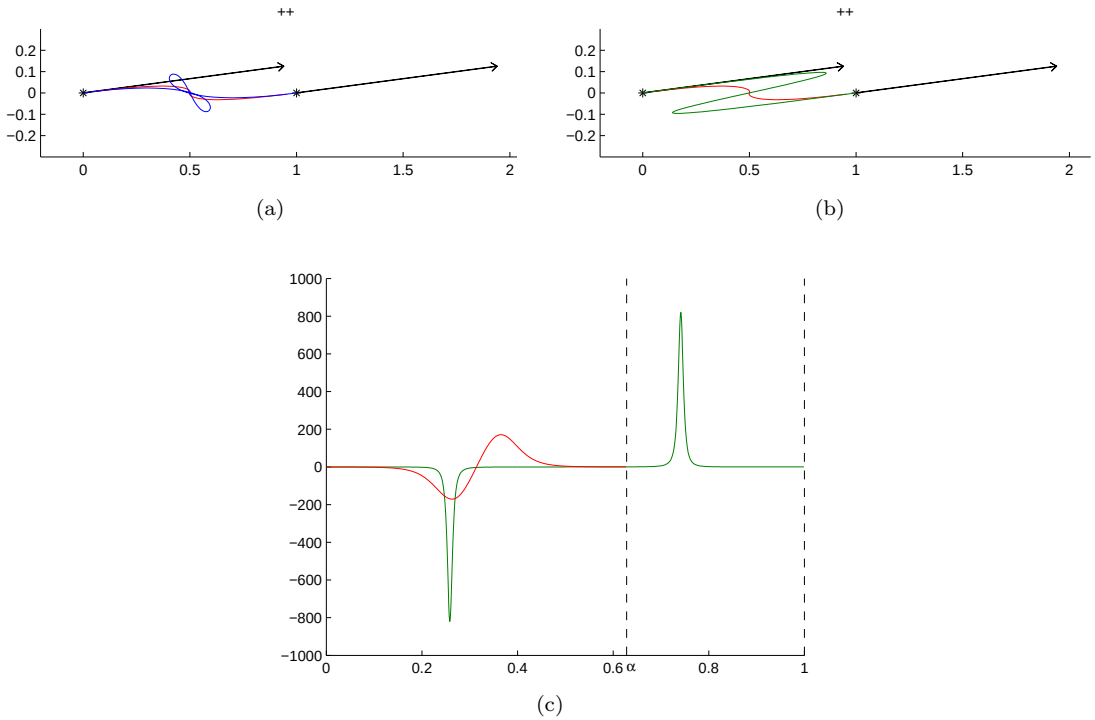

(a) (b) (c)

Fig. 13 In (a) and (b) the (++) ATPH interpolant to the end points $\mathbf{p}_0 = 0$, $\mathbf{p}_5 = 1$ and associated end derivatives $\mathbf{d}_0 = \mathbf{d}_2 = 7.5 + \mathrm{i}$ (plotted with a scale factor of $\frac{1}{8}$), obtained for $\alpha = \frac{\pi}{5}$, is drawn in red. The corresponding PH quintic interpolant (a) and the ordinary cubic interpolant (b) to the same data are displayed in blue and green, respectively. In (c) the curvature behaviour of the ATPH interpolant (red) and the cubic interpolant (green).

Hermite data requiring the associated end derivatives, $\mathbf{d}_0$ and $\mathbf{d}_2$, to vary in the open half-disk

$$\mathcal{D}_\alpha = \left\{ \mathbf{d} \in \mathbb{C} \,:\, \mathrm{Re}(\mathbf{d}(\overline{\mathbf{p}_5 - \mathbf{p}_0})) > 0 \text{ and } |\mathbf{d}| < \frac{3}{\alpha} |\mathbf{p}_5 - \mathbf{p}_0| \right\} \quad \text{with} \quad \alpha \in \left(0, \frac{2}{3}\pi\right). \tag{35}$$

This choice of $\mathcal{D}_\alpha$ does not constitute a limitation for the practical applications we have in mind. In the following we numerically show that the (++) ATPH interpolant always has a well-behaved tangent variation whenever $\mathbf{d}_0$, $\mathbf{d}_2$ are chosen in $\mathcal{D}_\alpha$. Such a conjecture allows us to assert that, whenever these Hermite data are prescribed, the (++) solution can be directly selected as the best ATPH interpolant, without explicitly constructing all the four solutions and comparing them.

Conjecture 1 If the Hermite end derivatives $\mathbf{d}_0$ and $\mathbf{d}_2$ lie within the domain $\mathcal{D}_\alpha$, the hodograph $\mathbf{x}'(t)$ of the (++) ATPH interpolant $\mathbf{x}(t)$ remains inside $\mathcal{D}_\alpha$ for all $t \in [0, \alpha]$ and $\alpha \in \left(0, \frac{2}{3}\pi\right)$.

Proof Without loss of generality, we choose the end points $\mathbf{p}_0 = 0$ and $\mathbf{p}_5 = 1$. We then recall that, for a general ATPH interpolant $\mathbf{x}(t)$, the hodograph is given by (27), *i.e.*

$$\mathbf{x}'(t) = \mathbf{w}^2(t) = \left(\mathbf{w}_0 \tilde{B}_0^2(t) + \mathbf{w}_1 \tilde{B}_1^2(t) + \mathbf{w}_2 \tilde{B}_2^2(t)\right)^2.$$

If we consider the (++) ATPH interpolant from (28), due to the fact that $\mathbf{x}'(0) = \mathbf{w}^2(0) = \mathbf{w}_0^2 = \mathbf{d}_0$ and $\mathbf{x}'(\alpha) = \mathbf{w}^2(\alpha) = \mathbf{w}_2^2 = \mathbf{d}_2$ with $\mathbf{d}_0, \mathbf{d}_2 \in \mathcal{D}_\alpha$, we have

$$\begin{aligned} \mathbf{w}_0 &= \sqrt{\mathbf{d}_0}, \\ \mathbf{w}_2 &= \sqrt{\mathbf{d}_2}, \\ \mathbf{w}_1 &= |\mathbf{d}_1|^{\frac{1}{2}}(\cos(\tfrac{\omega_1}{2}) + \mathrm{i}\sin(\tfrac{\omega_1}{2})) - \tfrac{n_0 - 6n_2}{4n_2(1+c_2)}(\mathbf{w}_0 + \mathbf{w}_2) = g(\mathbf{w}_0, \mathbf{w}_2), \end{aligned} \tag{36}$$

where $\sqrt{\mathbf{d}_i}$ for $i = 0, 2$ denotes the principal value of the complex square root, *i.e.*, with positive real part, and

$$\mathbf{d}_1 = \frac{1}{1+c_2}\left(\frac{4s_1^4}{n_2}(\mathbf{p}_4 - \mathbf{p}_1) + \frac{(n_0 - 6n_2)^2}{16n_2^2(1+c_2)}(\mathbf{w}_0 + \mathbf{w}_2)^2 - \mathbf{w}_0\mathbf{w}_2\right) \quad \text{with} \quad \omega_1 = \arg(\mathbf{d}_1).$$

To show that $\mathbf{x}'(t)$ is contained within $\mathcal{D}_\alpha$ for all $t \in [0, \alpha]$ and $\alpha \in (0, \frac{2}{3}\pi)$, we can verify that for all $t \in [0, \alpha]$ $\mathbf{w}(t)$ lies within the open set

$$\sqrt{\mathcal{D}_\alpha} = \left\{\mathbf{z} \in \mathbb{C} : \mathrm{Re}(\mathbf{z}) > |\mathrm{Im}(\mathbf{z})| \ \text{ and } \ |\mathbf{z}| < \sqrt{\frac{3}{\alpha}}\right\}, \qquad \text{with} \quad \alpha \in \left(0, \frac{2}{3}\pi\right).$$

This is a wedge of a disk of radius $\sqrt{\frac{3}{\alpha}}$, between angles $-\frac{\pi}{4}$ and $\frac{\pi}{4}$ about the x-axis. Following the proof in [12, Proposition 2], we apply the de Casteljau-like algorithm previously described in Section 2 for the evaluation of trigonometric Bézier curves over the space $\tilde{U}_2$, to split $\mathbf{w}(t)$ in correspondence to the parameter $t = \frac{\alpha}{2}$. From equation (3) we get that the control points of the two subcurves $\mathbf{w}_l(t)$, $\mathbf{w}_r(t)$ joining at such location are

$$\mathbf{w}_l(t) = \sqrt{\mathbf{x}_l'(t)} = \mathbf{w}_0\tilde{B}_0^2(t) + \mathbf{m}_{01}\tilde{B}_1^2(t) + \frac{1}{2}(\mathbf{m}_{01} + \mathbf{m}_{12})\tilde{B}_2^2(t),$$

$$\mathbf{w}_r(t) = \sqrt{\mathbf{x}_r'(t)} = \frac{1}{2}(\mathbf{m}_{01} + \mathbf{m}_{12})\tilde{B}_0^2(t) + \mathbf{m}_{12}\tilde{B}_1^2(t) + \mathbf{w}_2\tilde{B}_2^2(t),$$

where

$$\mathbf{m}_{01} = \frac{\cos(\frac{\alpha}{2})\mathbf{w}_1 + \mathbf{w}_0}{\cos(\frac{\alpha}{2}) + 1} \qquad \text{and} \qquad \mathbf{m}_{12} = \frac{\cos(\frac{\alpha}{2})\mathbf{w}_1 + \mathbf{w}_2}{\cos(\frac{\alpha}{2}) + 1}. \tag{37}$$

By the convexity of $\sqrt{\mathcal{D}_\alpha}$ and the convex hull property of the generalized Bézier curves built-upon the normalized B-basis $\tilde{B}_i^2(t)$, $i = 0, 1, 2$, it suffices to show that for arbitrary values of $\mathbf{w}_0$ and $\mathbf{w}_2$ in $\sqrt{\mathcal{D}_\alpha}$, $\mathbf{m}_{01}$ and $\mathbf{m}_{12}$ are also contained in $\sqrt{\mathcal{D}_\alpha}$. To this purpose, we use the *Minkowski geometric algebra* of complex sets [7,8] and a generalization of Minkowski sums and products by the concept of an *implicitly-defined set* $\mathcal{A} \odot_f \mathcal{B} = \{f(\mathbf{a}, \mathbf{b}) : \mathbf{a} \in \mathcal{A}, \mathbf{b} \in \mathcal{B}\}$, corresponding to a given bivariate function $f(\mathbf{a}, \mathbf{b})$ [8]. From (36) and (37) we have that the Bézier coefficients $\mathbf{m}_{01}$ and $\mathbf{m}_{12}$ can be regarded as complex-valued functions of values $\mathbf{w}_0$, $\mathbf{w}_2$ chosen from $\sqrt{\mathcal{D}_\alpha}$, *i.e.*

$$\mathbf{m}_{01} = f_0(\mathbf{w}_0, \mathbf{w}_2) = \frac{\cos(\frac{\alpha}{2})g(\mathbf{w}_0, \mathbf{w}_2) + \mathbf{w}_0}{\cos(\frac{\alpha}{2}) + 1}, \quad \mathbf{m}_{12} = f_1(\mathbf{w}_0, \mathbf{w}_2) = \frac{\cos(\frac{\alpha}{2})g(\mathbf{w}_0, \mathbf{w}_2) + \mathbf{w}_2}{\cos(\frac{\alpha}{2}) + 1}.$$

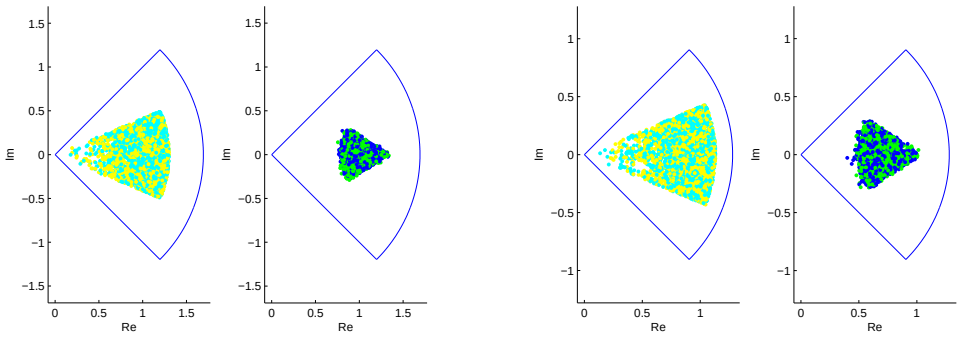

(a) $\alpha = \frac{\pi}{3}$ (b) $\alpha = \frac{7}{12}\pi$

Fig. 14 Visualization of random choices of $\mathbf{w}_0$, $\mathbf{w_2}$ in the domain $\sqrt{\mathcal{D}_\alpha}$ (left) and visualization of the hodograph control points $\mathbf{m}_{01}$ (green) and $\mathbf{m}_{12}$ (blue) lying inside the same domain (right), for $\alpha = \frac{\pi}{3}$(a) and $\alpha = \frac{7}{12}\pi$(b).

Therefore, the control points $\mathbf{m}_{01}$ and $\mathbf{m}_{12}$ lie in the region defined by

$$\sqrt{\mathcal{D}_\alpha} \odot_{f_i} \sqrt{\mathcal{D}_\alpha} = \{f_i(\mathbf{z}_1, \mathbf{z}_2) \,:\, \mathbf{z}_1 \in \sqrt{\mathcal{D}_\alpha},\, \mathbf{z}_2 \in \sqrt{\mathcal{D}_\alpha}\}\,, \quad i = 0, 1.$$

Although this implicitly-defined set does not allow a closed-form evaluation, as in the proof of [12, Proposition 2] we can evaluate it numerically, thus obtaining $\sqrt{\mathcal{D}_\alpha} \odot_{f_i} \sqrt{\mathcal{D}_\alpha} \subset \sqrt{\mathcal{D}_\alpha}$, for all $\alpha \in (0, \frac{2}{3}\pi)$. Figure 14 shows the result for some sample values of α in the interval. As a consequence, $\mathbf{w}(t)$ is entirely contained within $\sqrt{\mathcal{D}_\alpha}$ for all $\alpha \in (0, \frac{2}{3}\pi)$, and thus the hodograph $\mathbf{x}'(t) = \mathbf{w}^2(t)$ of the (++) ATPH interpolant $\mathbf{x}(t)$ lies within $\mathcal{D}_\alpha$ for all the same choices of α, which leads to the conclusion of the above conjecture. □

6 Construction of ATPH spirals

In this section we define *ATPH spirals* as Algebraic-Trigonometric Pythagorean Hodograph curves with monotone curvature, i.e., with no interior curvature extrema. Spiral segments are widely used in several practical applications such as, e.g., highway and railway design, or robot path planning. The control of the curvature behaviour is also desirable in many CAD and CAGD applications. While quintic PH curves with monotone curvature can be also obtained [6], the advantage of an ATPH spiral lies in the fact that it allows for higher flexibility and better curvature variation. In the next sections we will describe a general construction of ATPH spirals to be used as G^2 transition elements either between a line and a circle that do not intersect or between a pair of external circles.

6.1 ATPH spiral for designing a G^2 transition between a line and a circle

Let $\mathbf{x}(t) = \sum_{i=0}^{5} \mathbf{p}_i B_i^5(t)$, $t \in [0, \alpha]$ be an ATPH curve with control points $\mathbf{p}_i$, $i = 0, ..., 5$ as in (18)-(22), where $\mathbf{p}_0$ is a complex arbitrary integration constant and $\mathbf{w}_j = u_j + \mathrm{i}v_j = w_j e^{\mathrm{i}\theta_j}$, $j = 0, 1, 2$. Given two vectors $\mathbf{t}_0$ and $\mathbf{t}_\alpha$, in the following we define an ATPH spiral $\mathbf{x}(t)$ such that

(a) $\mathbf{x}(0) = \mathbf{p}_0$, $\mathbf{t}_0$ is the tangent at $t = 0$, $\kappa(0) = 0$;
(b) $\mathbf{t}_\alpha$ is the tangent at $t = \alpha$, $\kappa(\alpha) = \frac{1}{R}$ $(R > 0)$, $\kappa'(\alpha) = 0$;
(c) $\mathbf{x}(t)$ has monotonically increasing curvature, i.e., $\kappa'(t) > 0$ for all $t \in [0, \alpha]$.

The resulting algorithm turns out to be a modification of the one proposed in [6], based on polynomial PH quintics. Following the methodology used in [6], without loss of generality we assume $\mathbf{p}_0 = 0$. In this way $\mathbf{x}(0) = 0$. Moreover, we set $\mathbf{t}_0 = 1$ and $\mathbf{t}_\alpha = e^{\mathrm{i}\theta}$, with $0 < \theta < \pi$. Thus, being $\mathbf{x}'(t) = \mathbf{w}^2(t)$ with $\mathbf{w}(t)$ in (16), from the second condition in (a) we get $\mathbf{x}'(0) = \mathbf{w}_0^2 = w_0^2$ and from the first condition in (b) we obtain $\mathbf{x}'(\alpha) = \mathbf{w}_2^2 = w_2^2 e^{\mathrm{i}\theta}$. From these two equations we immediately have

$$\mathbf{w}_0 = w_0 \in \mathbb{R}\backslash\{0\} \qquad \text{and} \qquad \mathbf{w}_2 = w_2 e^{\mathrm{i}\frac{\theta}{2}}, \quad 0 < \theta < \pi, \;\; w_2 \in \mathbb{R}\backslash\{0\}. \tag{38}$$

Now, recalling that the (signed) curvature of the ATPH curve has the expression

$$\kappa(t) = 2\,\frac{\mathrm{Im}\Big(\overline{\mathbf{w}}(t)\,\mathbf{w}'(t)\Big)}{|\mathbf{w}(t)|^4}, \tag{39}$$

and $\mathbf{w}'(0) = \cot\left(\frac{\alpha}{2}\right)(\mathbf{w}_1 - \mathbf{w}_0)$, the value of $\kappa(0)$ can be simply written in the form $\kappa(0) = 2\,\cot\left(\frac{\alpha}{2}\right)\,\frac{\mathrm{Im}(\mathbf{w}_1)}{w_0^3}$. By requiring $\kappa(0) = 0$ (third condition in (a)) we thus get $\mathrm{Im}(\mathbf{w}_1) = 0$, i.e.,

$$\mathbf{w}_1 = w_1 \in \mathbb{R}\backslash\{0\}. \tag{40}$$

On the other hand, for the endpoint $t = \alpha$, being $\mathbf{w}'(\alpha) = \cot\left(\frac{\alpha}{2}\right)(\mathbf{w}_2 - \mathbf{w}_1)$, and substituting $\mathbf{w}_1 = w_1$, from (39) we obtain $\kappa(\alpha) = 2\,\cot\left(\frac{\alpha}{2}\right)\,\frac{w_1}{w_2^3}\,\sin\left(\frac{\theta}{2}\right)$. Therefore, requiring that $\kappa(\alpha) = \frac{1}{R}$, with $R > 0$, (second condition in (b)) we find $w_1 = \frac{w_2^3\,\tan\left(\frac{\alpha}{2}\right)}{2R\sin\left(\frac{\theta}{2}\right)}$. We now proceed by imposing the condition $\kappa'(\alpha) = 0$ (the last of (b)). Since

$$\kappa'(t) = 2\frac{\mathrm{Im}\left(\overline{\mathbf{w}}^2(t)\,(\mathbf{w}(t)\mathbf{w}''(t) - 2\mathbf{w}'^2(t))\right)}{|\mathbf{w}(t)|^6} \quad \text{and} \quad \mathbf{w}''(\alpha) = \frac{1}{1-\cos(\alpha)}\Big(\mathbf{w}_0 - (1+\cos(\alpha))\mathbf{w}_1 + \cos(\alpha)\mathbf{w}_2\Big),$$

then setting $\kappa'(\alpha) = 0$ gives $\mathrm{Im}\Big(3(1+\cos(\alpha))\,|\mathbf{w}_2|^2\mathbf{w}_1\overline{\mathbf{w}}_2 + |\mathbf{w}_2|^2\mathbf{w}_0\overline{\mathbf{w}}_2 - 2(1+\cos(\alpha))\,\mathbf{w}_1^2\overline{\mathbf{w}}_2^2\Big) = 0$, and inserting the values of $\mathbf{w}_j$, $j = 0, 1, 2$, from (38), (40) the last equation provides

$$w_0 = \frac{w_2^3\Big(2(1-\cos(\alpha))w_2^2\cos\left(\frac{\theta}{2}\right) - 3R\sin(\alpha)\sin\left(\frac{\theta}{2}\right)\Big)}{2R^2\sin^2\left(\frac{\theta}{2}\right)}.$$

Now, introducing the notation $M = \frac{w_2^2}{R}$, we can rewrite the expressions for the coefficients $\mathbf{w}_j$, $j = 0, 1, 2$ in terms of the parameter M as follows:

$$\begin{aligned}
\mathbf{w}_0 &= w_0 = \sqrt{RM^3}\,\frac{2(1-\cos(\alpha))M\cos\left(\frac{\theta}{2}\right) - 3\sin(\alpha)\sin\left(\frac{\theta}{2}\right)}{2\sin^2\left(\frac{\theta}{2}\right)},\\
\mathbf{w}_1 &= w_1 = \sqrt{RM^3}\,\frac{1-\cos(\alpha)}{2\sin(\alpha)\sin\left(\frac{\theta}{2}\right)},\\
\mathbf{w}_2 &= \sqrt{RM}\,\Big(\cos\left(\tfrac{\theta}{2}\right) + \mathrm{i}\sin\left(\tfrac{\theta}{2}\right)\Big).
\end{aligned}$$

We now still have to satisfy the additional requirement $\kappa'(t) > 0$ for all $t \in [0, \alpha]$ (condition (c)). This will provide a lower bound on the admissible values of w_2. Looking at the formula of $\kappa'(t)$, it is evident that the problem reduces to study a sufficient condition on w_2 that guarantees

$$\mathrm{Im}\left(\overline{\mathbf{w}}^2(t)\,(\mathbf{w}(t)\mathbf{w}''(t) - 2\mathbf{w}'^2(t))\right) > 0 \qquad \forall t \in [0, \alpha]. \tag{41}$$

Let us start by observing that we can write

$$\mathrm{Im}\left(\overline{\mathbf{w}}^2(t)\,(\mathbf{w}(t)\mathbf{w}''(t) - 2\mathbf{w}'^2(t))\right) = \frac{M^3\,R^2}{24\tilde{s}^5 s_1 c_1}\,\sum_{i=0}^{6} b_i\tilde{B}_i^6(t),$$

where $\{\tilde{B}_i^6(t)\}_{i=0,\ldots,6}$ is the normalized B-basis in (2) and

$$\begin{aligned}
b_0 &= 12M^2 s_1^2 c_1\,(2Ms_1\tilde{c} - 3\tilde{s}c_1)^3\,,\\
b_1 &= 2M^2 s_1^2\,(2Ms_1\tilde{c} - 3\tilde{s}c_1)^2\,\left(16M\tilde{c}s_1c_1 - \tilde{s}(24c_1^2+1)\right),\\
b_2 &= \tfrac{4Ms_1c_1}{4c_1^2+1}\Big(56M^4 s_1^4\tilde{c}^3 - 200M^3 s_1^3 c_1\tilde{s}\tilde{c}^2 + 6M^2 s_1^2\tilde{c}\tilde{s}^2(37c_1^2 - 4\tilde{c}^2 - 1)\\
&\qquad +9Ms_1c_1\tilde{s}^3(8s_1^2 - 8\tilde{s}^2 + 1) - 54c_1^2\tilde{c}\tilde{s}^4\Big),\\
b_3 &= \tfrac{3Ms_1\tilde{s}}{3+2c_1^2}\Big(56M^3 s_1^3\tilde{c}^2 - 156M^2 c_1 s_1^2\tilde{c}\tilde{s} + Ms_1\tilde{s}^2(108c_1^2 - 24\tilde{c}^2 - 1) + 36c_1\tilde{c}\tilde{s}^3\Big),\\
b_4 &= \tfrac{4c_1\tilde{s}^2}{4c_1^2+1}\Big(6M^3 s_1^3\tilde{c}(4\tilde{c}^2+3) - 2M^2 s_1^2 c_1\tilde{s}(42\tilde{c}^2+13) + 18Ms_1(4c_1^2-1)\tilde{s}^2\tilde{c} + 21c_1\tilde{s}^3\Big),\\
b_5 &= 2\tilde{s}^3\Big(2M^2 s_1^2(6\tilde{c}^2+1) - 36Ms_1c_1\tilde{s}\tilde{c} + 3(8c_1^2-1)\tilde{s}^2\Big),\\
b_6 &= 0,
\end{aligned}$$

with $\tilde{s} := \sin\left(\frac{\theta}{2}\right)$, $\tilde{c} := \cos\left(\frac{\theta}{2}\right)$ and s_1, c_1 from (4).

Remark 3 Note that the Bézier coefficient $b_6 = 0$ agrees with the requirement $\kappa'(\alpha) = 0$.

Thus, if we assume $0 < \alpha < \pi/2$ and $0 < \theta < \pi$, it turns out that any arbitrary choice of w_2 satisfying the inequality $w_2 > \sqrt{k^* R \tan\left(\frac{\theta}{2}\right)}$ with $k^* = \frac{5}{2}\cot\left(\frac{\alpha}{2}\right) - \cot(\alpha)$, guarantees that all the coefficients b_i, $i = 0, ..., 5$ are strictly positive and therefore (41) is satisfied. As a consequence, for any arbitrary $k > k^*$ we can equivalently set $w_2 = \sqrt{k\, R \tan\left(\frac{\theta}{2}\right)}$ and rewrite the coefficients $\mathbf{w}_j$, $j = 0, 1, 2$ in terms of the parameter k as follows:

$$\begin{aligned}
\mathbf{w}_0 &= \sqrt{kR\tan\left(\tfrac{\theta}{2}\right)}\ \tfrac{k}{2}\Big(2(1-c_2)k - 3s_2\Big)\ \sec\left(\tfrac{\theta}{2}\right),\\
\mathbf{w}_1 &= \sqrt{kR\tan\left(\tfrac{\theta}{2}\right)}\ \tfrac{k}{2}\ \tfrac{s_1}{c_1}\ \sec\left(\tfrac{\theta}{2}\right),\\
\mathbf{w}_2 &= \sqrt{kR\tan\left(\tfrac{\theta}{2}\right)}\ \left(\cos\left(\tfrac{\theta}{2}\right) + \mathrm{i}\sin\left(\tfrac{\theta}{2}\right)\right),
\end{aligned} \tag{42}$$

with s_i, c_i, $i = 1, 2$ from (4).

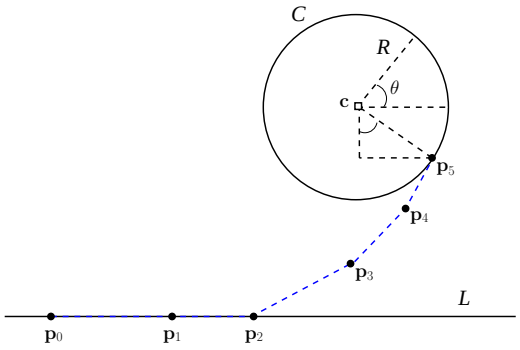

Fig. 15 Geometrical parameters of an ATPH spiral used as a G^2 join between a line L and a circle C.

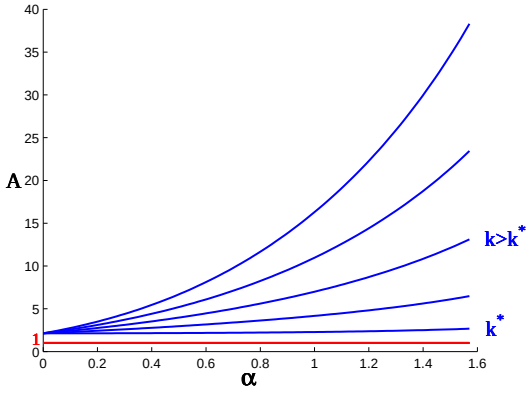

Fig. 16 Behaviour of $A(k, \alpha)$ for $\alpha \in (0, \pi/2)$.

Now, if we want to exploit the ATPH spiral satisfying the above conditions (a),(b),(c) to connect G^2 continuously a line L and a circle C that do not intersect, without loss of generality we can assume L to be the x-axis with the transition curve starting at $\mathbf{p}_0 = x_0$ and take C of radius R and center $\mathbf{c} = l + \mathrm{i}h$ with $h > R$. We observe that, the requirement $\kappa'(\alpha) = 0$ included in (b), indeed implies a G^3 contact of the ATPH spiral with the circle C, while the contact with the line L is only G^2.
Measuring the angular position θ on the circle in the anticlockwise sense from a perpendicular dropped to L from $\mathbf{c}$ (see Figure 15), the transition curve is identified by the requirement $\mathrm{Im}(\mathbf{p}_5 - \mathbf{p}_0) = h - R\cos(\theta)$. Using standard trigonometric relations, the last equation leads to

$$Q(\cos(\theta)) := a_2 \cos^2(\theta) + a_1 \cos(\theta) + a_0 = 0, \tag{43}$$

where

$$\begin{aligned}
a_0 &= 4Rc_1n_2(1-c_2)k^3 + Rs_1(n_0 - 6n_2(c_2+2))k^2 + Rc_1n_0k - 16c_1s_1^4h,\\
a_1 &= 4Rc_1n_2(c_2-1)k^3 + Rs_1(6n_2(c_2+2) - n_0)k^2 + 16c_1s_1^4(R-h),\\
a_2 &= -Rc_1(kn_0 - 16s_1^4).
\end{aligned} \tag{44}$$

Since $Q(0) = a_0 = Rk\left(4c_1n_2(1-c_2)k^2 + s_1(n_0 - 6n_2(c_2+2))k + c_1n_0\right) - 16c_1s_1^4h$ and $Q(1) = a_2 + a_1 + a_0 = 32c_1s_1^4(R-h)$, being $0 < \alpha < \pi/2$ and $0 < \theta < \pi$, when h satisfies

$$R < h < A(k,\alpha)\, R \quad \text{with} \quad A(k,\alpha) = k\,\frac{(4c_1n_2(1-c_2)k^2 + s_1(n_0 - 6n_2(c_2+2))k + c_1n_0)}{16c_1s_1^4}, \tag{45}$$

we have $Q(0) > 0$ and $Q(1) < 0$, so that equation (43) has a unique root satisfying $\cos(\theta) \in (0,1)$. Note that, when $k = k^* \left(= \frac{5}{2}\cot\left(\frac{\alpha}{2}\right) - \cot(\alpha)\right)$, then $A(k,\alpha) > 1$ for all $\alpha \in \left(0, \frac{\pi}{2}\right)$ and $A(k,\alpha)$ is monotonically increasing for $k > k^*$ (see Figure 16). In this way, for any value of $\alpha \in (0, \pi/2)$, we can make the upper bound on h as large as we want by taking k sufficiently large. Remember also that, if we denote by $\overline{k}$ the value such that $A(\overline{k},\alpha) = \frac{h}{R}$, we need to certainly choose $k > \max(k^*, \overline{k})$ in order to satisfy (45). See Figure 17 for an illustrative example of this situation.

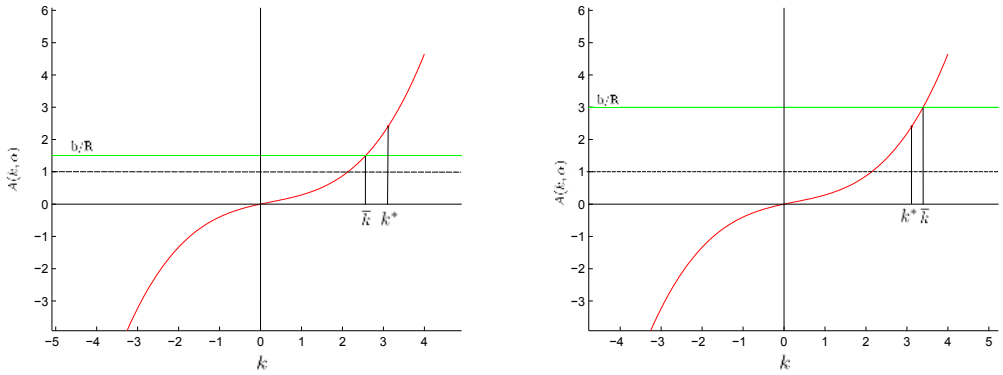

Fig. 17 Behaviour of $A(k,\alpha)$ for $\alpha = \frac{2}{5}\pi$ and $R = 2$, $h = 3$ (left), $R = 1$, $h = 3$ (right).

For the sake of clarity, we conclude by summarizing the steps of the algorithm to draw an ATPH spiral to connect G^2 continuously a line L corresponding to the x-axis and a circle C of radius $R > 0$ and center (l,h) with $h > R$.

Algorithm

Input: l, $h > 0$, $R \in (0,h)$, $\alpha \in (0,\pi/2)$.

1. Choose k such that inequality (45) is satisfied;
2. Compute a_0, a_1, a_2 in (44);
3. Determine $\theta \in (0,\pi)$ by solving (43);
4. Work out the values of $\mathbf{w}_0, \mathbf{w}_1, \mathbf{w}_2$ given in (42);
5. Determine x_0 by solving the equation $\mathrm{Re}(\mathbf{p}_5 - \mathbf{p}_0) = l + R\sin(\theta) - x_0$.

Output: Control points $\mathbf{p}_0 = x_0$, $\mathbf{p}_i$, $i = 1,...,4$, $\mathbf{p}_5 = l + R\sin(\theta) + \mathrm{i}(h - R\cos(\theta))$ of the ATPH spiral connecting L and C.

As an application example of the previously developed constructive strategy we consider the following choices: $R = 2$, $l = 4$ and $h = 3$. In Figure 18 we display the obtained ATPH spiral for $\alpha = \frac{\pi}{5}$, $\alpha = \frac{\pi}{3}$ and $\alpha = \frac{2}{5}\pi$ when $k = k^*$, and in Figure 19 the corresponding quintic PH spiral for which k satisfies $R < h < \frac{2k^3 - 3k^2 + 12k}{60} R$ (see [6]). In Figure 20 we plot the behaviour of $\kappa'(t)$ for the ATPH spirals in Figure 18 and the quintic PH spiral in Figure 19. As we can see, for an ATPH spiral (black), the maximum of the function $\kappa'(t)$ is decreasing for increasing values of α, while for a PH spiral (blue) it is obviously a fixed value. As a consequence the parameter α can be suitably selected to control the curvature variation and ensure the most desired behaviour of the ATPH spiral.

Furthermore, by evaluating the arc length of the ATPH spiral over the interval $[0,\alpha]$ from formula (33) with $\mathbf{w}_0, \mathbf{w}_1, \mathbf{w}_2$ in (42), we can obtain the length of the ATPH spiral

$$S_\alpha = k\,\frac{R}{4(c_2-1)^2}\,\tan\left(\frac{\theta}{2}\right)\Big[\Big(2(1-c_2)n_0k^2 + 4\left((1-c_2)(3s_2^2 + 10c_2 + 14) - 12\alpha s_2\right)k + (47c_2 + 49)\alpha$$
$$+3s_2(3c_2^2 - 11c_2 - 24)\Big)k^2 s_1^2 \sec^2\left(\tfrac{\theta}{2}\right) - 4(c_2-1)n_2k^2 - 2\Big((c_2-1)(c_2+5) + 3s_2(n_2+\alpha)\Big)k + n_0\Big],$$

with s_i, c_i, $i = 1,2$ from (4) and n_0, n_2 from (5). Observe that, the parameter k can be selected such that the total arc length S_α assumes a specified value. This requires to solve a polynomial equation

of degree 5. Although this is possible also in the polynomial case presented in [6], if using an ATPH spiral, once the value of k has been fixed, we still have another free parameter α that can be used for other purposes.

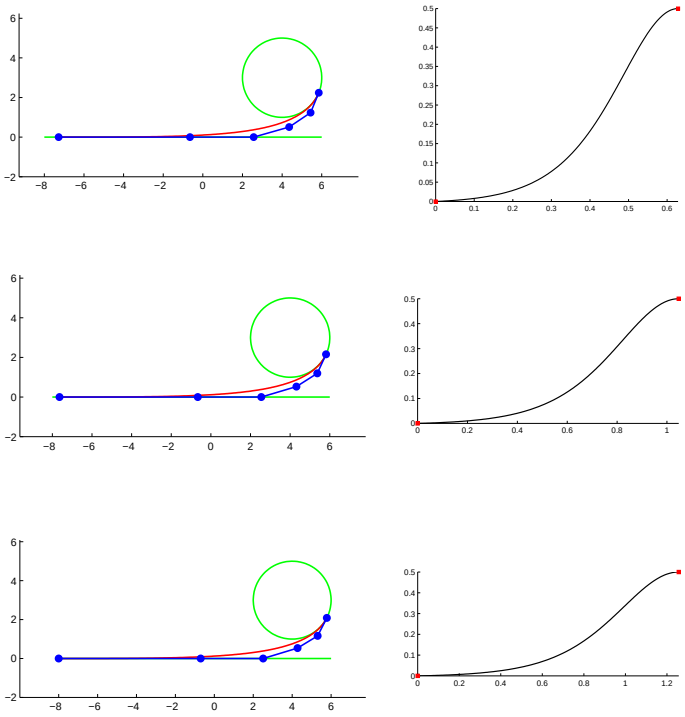

Fig. 18 First column: ATPH spirals for $\alpha = \frac{\pi}{5}, \frac{\pi}{3}, \frac{2}{5}\pi$, where $k = k^*$. Second column: corresponding curvature plots.

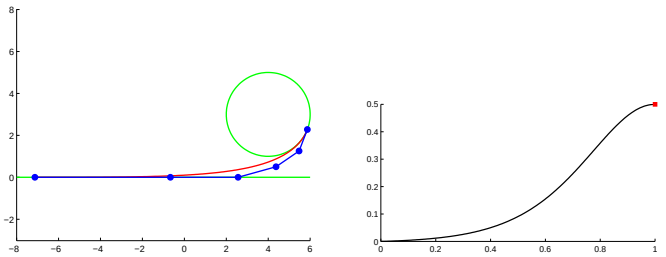

Fig. 19 Quintic PH spiral for $k = 4$ (left) and its curvature plot (right).

6.2 S-shaped ATPH spiral for designing a G^2 transition between two circles

In this section we consider the problem of designing an S-shaped ATPH spiral to join two given circles Ω_0, Ω_1 with centers $\boldsymbol{C}_0$, $\boldsymbol{C}_1$ and radii r_0, r_1, such that at both points of contact G^2 continuity is ensured. We denote the distance between the centers of the two circles by

$$r = |\boldsymbol{C}_1 - \boldsymbol{C}_0|, \tag{46}$$

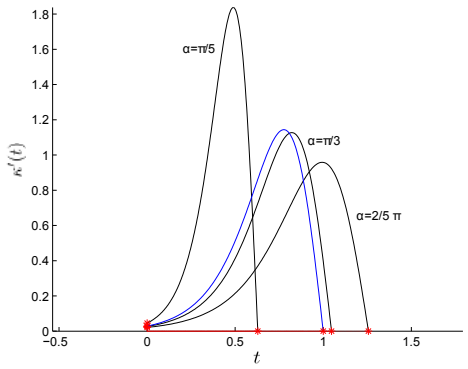

Fig. 20 Behaviour of $\kappa'(t)$ for the ATPH spirals in Figure 18 with $\alpha = \frac{\pi}{5}, \frac{\pi}{3}, \frac{2}{5}\pi$ (black) and for the quintic PH spiral in Figure 19 (blue).

and we define $r_1 = \frac{r_0}{\mu^3}$, where $\mu \geq 1$. Moreover, without loss of generality (after suitable translation, rotation and reflection), for the starting point of the ATPH curve we can assume $\mathbf{p}_0 = 0$, as well as the curvature at the starting point being 1 (i.e. $r_0 = 1$), $\mathbf{p}_1$ lying on the positive x-axis ($\mathrm{Re}(\mathbf{p}_1) > 0$), the larger circle having the center $\boldsymbol{C}_0 = \mathrm{i}$, and the end point $\mathbf{p}_5$ lying above the x-axis ($\mathrm{Im}(\mathbf{p}_5) > 0$). We then denote by θ and $2n\theta$ the angles from $\mathbf{p}_1 - \mathbf{p}_0$ to $\mathbf{p}_2 - \mathbf{p}_1$ and from $\mathbf{p}_1 - \mathbf{p}_0$ to $\mathbf{p}_5 - \mathbf{p}_4$, respectively (see Figure 21). By construction, it turns out that θ and $2n\theta$ may vary at most between 0 and $\frac{\pi}{2}$.

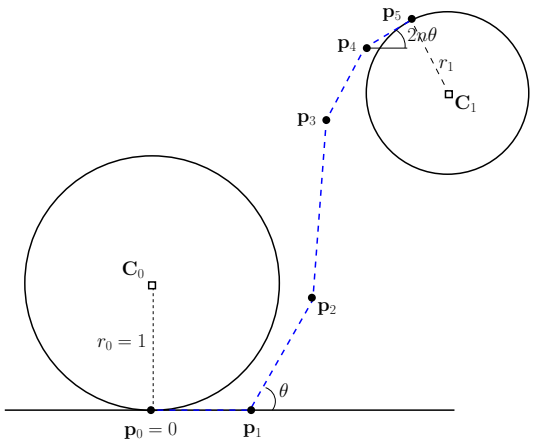

Fig. 21 Geometrical parameters of an S-shaped ATPH spiral used as G^2 connection between two external circles.

Summarizing, our goal is to define an S-shaped ATPH spiral that satisfies all the following requirements:

(i) $\mathbf{x}(0) = \mathbf{p}_0 = 0$
(ii) $\mathbf{t}_0 = 1$ is the tangent at $t = 0$ (i.e., $\mathbf{x}'(0) \parallel 1$)
(iii) $\mathbf{t}_\alpha = e^{2\mathrm{i}n\theta}$ is the tangent at $t = \alpha$ (i.e., $\mathbf{x}'(\alpha) \parallel (\cos(2n\theta) + \mathrm{i}\sin(2n\theta))$)
(iv) $(\mathbf{p}_2 - \mathbf{p}_1) \parallel (\cos(\theta) + \mathrm{i}\sin(\theta))$
(v) $(\kappa(0), \kappa(\alpha)) = (1, -\mu^3)$
(vi) $\mathbf{x}(t)$ has monotonously decreasing curvature, i.e. $\kappa'(t) < 0$ for all $t \in [0, \alpha]$.

By Kneser's theorem [10], it follows that a single S-shaped segment cannot have monotone curvature both in case of tangent and intersecting circles, as well as when one is contained into the other. Thus, we can draw S-shaped ATPH transitions satisfying the above requirements, only under the condition $r_0 + r_1 < r$. As in the previous section, in order to determine the ATPH spiral solving the above problem, we need to work out its complex coefficients $\mathbf{w}_j$, $j = 0, 1, 2$. To this end we suitably modify the methodology presented in [11] for the construction of its polynomial counterpart. First of all, recalling that $\mathbf{x}'(t) = \mathbf{w}^2(t)$, from (ii) and (iii) we obtain respectively $\mathbf{w}_0 = w_0 \in \mathbb{R}\backslash\{0\}$ and

$\mathbf{w}_2 = w_2\, e^{\mathrm{i}n\theta}$, $w_2 \in \mathbb{R}\backslash\{0\}$. Then, being $\mathbf{p}_2 - \mathbf{p}_1 = \frac{n_0-6n_2}{8s_1^4}\,\mathbf{w}_0\mathbf{w}_1$ with $\mathbf{w}_0 = w_0$, $\mathbf{w}_1 = w_1 e^{\mathrm{i}\theta_1}$ and $w_0, w_1 \in \mathbb{R}\backslash\{0\}$, from (iv) we immediately get $\theta_1 = \theta$. Before imposing condition (v), we recall once again that the (signed) curvature of the ATPH curve has the expression in (39). Thus, by requiring $\kappa(0) = 1$, we obtain $w_1 = \frac{w_0^3}{2\sin(\theta)}\tan\left(\frac{\alpha}{2}\right)$ and then $\mathbf{w}_1 = \frac{w_0^3}{2}\tan\left(\frac{\alpha}{2}\right)(\cot(\theta)+\mathrm{i})$. On the other hand, for the endpoint $t = \alpha$, condition $\kappa(\alpha) = -\mu^3$ leads to $w_2 = \frac{w_0}{\mu}\sqrt[3]{\frac{\sin((1-n)\theta)}{\sin\theta}}$. In conclusion, after introducing the notation

$$h = w_0^2, \qquad \varsigma = \frac{\cos(n\theta)}{\mu}\sqrt[3]{\frac{\sin((1-n)\theta)}{\sin\theta}}, \tag{47}$$

we can rewrite the coefficients $\mathbf{w}_j$, $j = 0, 1, 2$ in terms of h and ς as follows:

$$\begin{aligned} \mathbf{w}_0 &= \sqrt{h} \\ \mathbf{w}_1 &= \sqrt{h}\,\tfrac{h}{2}\tan\left(\tfrac{\alpha}{2}\right)\cot(\theta) + \mathrm{i}\sqrt{h}\,\tfrac{h}{2}\tan\left(\tfrac{\alpha}{2}\right) \\ \mathbf{w}_2 &= \sqrt{h}\,\varsigma + \mathrm{i}\sqrt{h}\,\varsigma\tan(n\theta). \end{aligned} \tag{48}$$

Thus, since $h, n, \mu, \theta, \alpha$ are free parameters, it turns out that there exists a whole family of ATPH curves $\mathbf{x}(t)$ satisfying the conditions (i)-(v). From (18)-(22) with $\mathbf{p}_0 = 0$ we obtain

$$\mathbf{p}_5 = \frac{n_0}{16s_1^4}(\mathbf{w}_0^2 + \mathbf{w}_2^2) + \frac{n_0 - 6n_2}{8s_1^4}\mathbf{w}_1(\mathbf{w}_0 + \mathbf{w}_2) + \frac{n_2}{4s_1^4}\left((1+c_2)\mathbf{w}_1^2 + \mathbf{w}_0\mathbf{w}_2\right),$$

where $\mathbf{w}_0, \mathbf{w}_1, \mathbf{w}_2$ are given by (48). Also taking into account that the coordinates of the centers of the two circles are $\boldsymbol{C}_0 = \mathbf{p}_0 + r_0\,(0,1) = (0,1)$ and $\boldsymbol{C}_1 = \mathbf{p}_5 + r_1\,(\sin(2n\theta), -\cos(2n\theta)) =: (p(h), q(h))$, having denoted by r the distance between $\boldsymbol{C}_0$ and $\boldsymbol{C}_1$, condition (46) determines a polynomial equation $f(h) = 0$ given by $f(h) = (p(h))^2 + (q(h)-1)^2 - r^2$. Therefore, for any fixed value of r, h needs to be determined by solving the polynomial equation $f(h) = 0$. Following the reasoning in [11] we can show the existence of a positive solution of $f(h) = 0$, which guarantees the existence of the ATPH spiral. It is easy to see that, if we further assume $\mu \geq 1.5$, this solution is also unique. Finally, considering requirement (vi), $\kappa'(t) < 0$ for all $t \in [0, \alpha]$, further restrictions on the admissible values of the free parameters α, θ, n, μ are obtained. Looking at the formula of $\kappa'(t)$, it is evident that the problem reduces to study sufficient conditions on the free parameters that ensure $\mathrm{Im}\left(\overline{\mathbf{w}}^2(t)\,(\mathbf{w}(t)\mathbf{w}''(t) - 2\mathbf{w}'^2(t))\right) < 0$ for all $t \in [0, \alpha]$. Writing $\mathrm{Im}\left(\overline{\mathbf{w}}^2(t)\,(\mathbf{w}(t)\mathbf{w}''(t) - 2\mathbf{w}'^2(t))\right)$ as a trigonometric Bézier in the space $\tilde{U}_6$, it is easy to see that this turns out to be negative for all $\alpha \in (0, \frac{\pi}{2})$ and considering the following restrictions on the remaining free parameters: $\theta \in (0, \pi/4]$, $n \in (0, 1/2)$, $\mu \in [1, 5]$.

As an application example of the proposed strategy for the construction of S-shaped ATPH spirals, we consider the following choice: $r_0 = 1$, $\mu = \sqrt[3]{2}$, $r_1 = \frac{1}{2}$, $r = 2$, $n = \frac{1}{3}$, $\theta = \frac{\pi}{5}$. In Figure 22(a), from top to bottom, we display the quintic PH spiral in [11] and the ATPH spirals with $\alpha = \frac{7}{24}\pi$ and $\alpha = \frac{5}{12}\pi$, obtained from the above data. Note that, although the quintic PH curve in Figure 22 (b) has monotone curvature, in general the S-shaped transition elements constructed in [11] do not guarantee the fulfillment of condition (vi). Moreover, from Figure 22 we can see that the additional free parameter α included in the ATPH approach can be used either to modify the location of the second point of contact of the spiral or to adjust the curvature profile and/or curvature variation of the spiral (see Figure 23).

7 Conclusions

In this article we have presented a trigonometric analogue of the Pythagorean Hodograph quintic, featured by the properties of possessing a closed-form representation of its arc–length and a rational algebraic-trigonometric representation of its offset curves. Slightly more cumbersome in its representation than its polynomial counterpart, it constitutes an interesting and powerful complement of the well-known polynomial PH quintics as shown at hand of the solution of several practical interpolation problems. After introducing a complex representation of the novel class of Algebraic–Trigonometric PH curves (called for short ATPH curves), ATPH curves that interpolate given end points and associated end derivatives have been constructed, as well as ATPH curves of monotone curvature joining

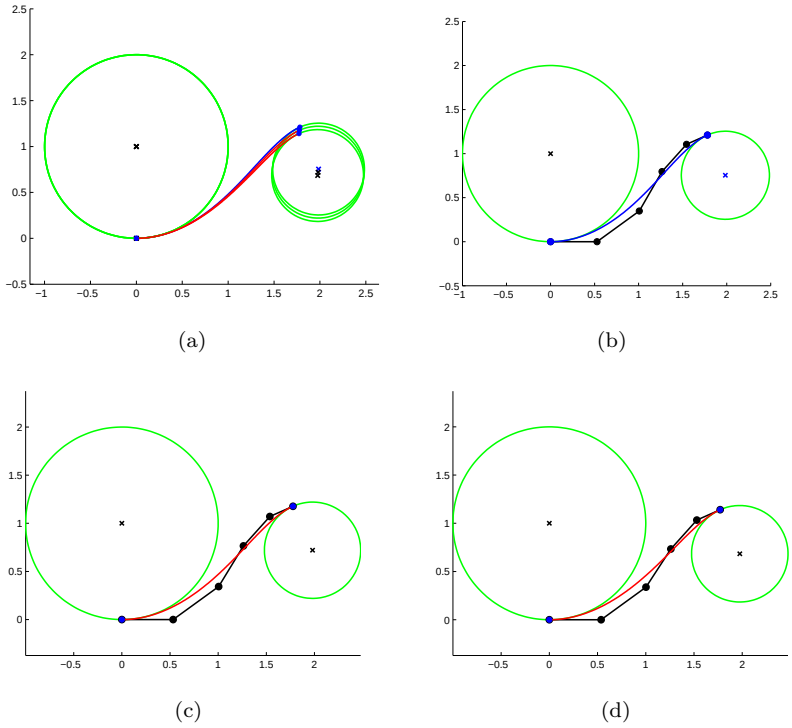

Fig. 22 (a) From top to bottom: S-shaped quintic PH spiral in [11] (blue) and S-shaped ATPH spirals with $\alpha = \frac{7}{24}\pi, \frac{5}{12}\pi$ (red). The control polygon for the S-shaped quintic PH spiral is displayed in (b) and that of the S-shaped ATPH spiral with $\alpha = \frac{7}{24}\pi$ and $\alpha = \frac{5}{12}\pi$ in (c) and (d) respectively.

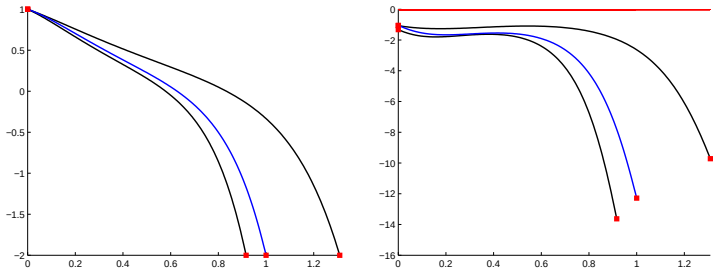

Fig. 23 Behaviour of $\kappa(t)$ (left) and $\kappa'(t)$ (right) for the S-shaped spirals in Fig. 22. From top to bottom the functions concerning the ATPH spiral with $\alpha = \frac{5}{12}\pi$, the quintic PH spiral in [11] (blue) and the ATPH spiral with $\alpha = \frac{7}{24}\pi$.

G^2-continuously basic elements such as line segments and circles. In both application contexts we have shown that the ATPH interpolants complement favorably their polynomial PH counterparts since, thanks to the shape parameter α, the user may choose the most appropriate interpolant out of a one-parameter family of solutions. In particular, concerning the C^1 Hermite interpolation problem, we have seen that, although there exist Hermite data such that all possible polynomial PH solutions manifest undesired self-intersections, ATPH interpolants constructed from the same information turn out to be free of loops if the free parameter α is suitably selected. Moreover, the free parameter α can be also conveniently exploited either to improve the curvature behaviour of ATPH spirals joining G^2-continuously a line and a circle, or to adjust the location of the second point of contact of the spiral, as well as the curvature profile and/or variation in the case of S-shaped spirals joining G^2-continuously a pair of external circles.

Acknowledgements

The authors are grateful to the anonymous referees for their useful comments that helped to improve the paper. Laura Saini acknowledges the financial support received for her PhD work from the Nord Pas de Calais Région (France) and the University of Valenciennes.

References

1. Carnicer, J.M., Pena, J.M.: Totally positive bases for shape preserving curve design and optimality of B-splines. Comput. Aided Geom. Design 11, 633-654 (1994)
2. Carnicer, J.M., Mainar, E., Pena, J.M.: Critical length for design purposes and extended Chebyshev spaces. Constr. Approx. 20, 55-71 (2004)
3. Farouki, R.T., Sakkalis, T.: Pythagorean hodographs. IBM J. Res. Develop. 34, 736-752 (1990)
4. Farouki, R.T. The conformal map $z \to z^2$ of the hodograph plane. Comput. Aided Geom. Design 11, 363-390 (1994)
5. Farouki, R.T., Neff, C.A.: Hermite interpolation by pythagorean hodograph quintics. Math. Comp. 64(212), 1589-1609 (1995)
6. Farouki, R.T.: Pythagorean-hodograph quintic transition curves of monotone curvature. Computer-Aided Design 29(9), 601-606 (1997)
7. Farouki, R.T., Moon, H.P., Ravani, B.: Minkowski geometric algebra of complex sets. Geometriae Dedicata (2000)
8. Farouki, R.T., Moon, H.P., Ravani, B.: Algorithms for Minkowski products and implicitly-defined complex sets. Adv. Comput. Math. 13, 199-229 (2000)
9. Farouki, R.T.: Pythagorean-Hodograph Curves: Algebra and Geometry Inseparable. Springer-Verlag, Berlin Heidelberg, 2008
10. Guggenheimer, H.: Differential Geometry. McGrawHill, New York, (1963)
11. Habib, Z., Sakai, M.: Transition between concentric or tangent circles with a single segment of G^2 PH quintic curve. Comput. Aided Geom. Design 25, 247-257 (2008)
12. Moon, H.P., Farouki, R.T., Choi, H.I.: Construction and shape analysis of PH quintic Hermite interpolants. Computer-Aided Design 18, 93-115 (2001)
13. Mainar, E., Peña, J.M.: Corner cutting algorithms associated with optimal shape preserving representations. Comput. Aided Geom. Design 16, 883-906 (1999)
14. Mainar, E., Peña, J.M., Sánchez-Reyes, J.: Shape preserving alternatives to the rational Bézier model. Comput. Aided Geom. Design 18, 37-60 (2001)
15. Mainar, E., Peña, J.M.: A general class of Bernstein-like bases. Computers and Mathematics with Applications 53, 1686-1703 (2007)
16. Mainar, E., Peña, J.M.: Optimal bases for a class of mixed spaces and their associated spline spaces. Computers and Mathematics with Applications 59, 1509-1523 (2010)
17. Sánchez-Reyes, J.: Harmonic rational Bézier curves, p-Bézier curves and trigonometric polynomials. Comput. Aided Geom. Design 15, 909-923 (1998)
18. Sasaki, T., Suzuki, M.: Three new algorithms for multivariate polynomial GCD. J. Symbolic Computation 13, 395-411 (1992)